NAVAL POSTGRADUATE SCHOOL

MONTEREY, CALIFORNIA

THESIS

A THREE DEGREES OF FREEDOM TEST BED FOR NANOSATELLITE AND CUBESAT ATTITUDE DYNAMICS, DETERMINATION, AND CONTROL

by

David M. Meissner

December 2009

Thesis Co-Advisors: Marcello Romano
Riccardo Bevilacqua

Approved for public release; distribution is unlimited

REPORT DOCUMENTATION PAGE		Form Approved OMB No. 0704-0188

1. AGENCY USE ONLY *(Leave blank)*	2. REPORT DATE December 2009	3. REPORT TYPE AND DATES COVERED Master's Thesis

4. TITLE AND SUBTITLE A Three Degrees of Freedom Test Bed for Nanosatellite and CubeSat Attitude Dynamics, Determination, and Control	5. FUNDING NUMBERS
6. AUTHOR(S) David M. Meissner	
7. PERFORMING ORGANIZATION NAME(S) AND ADDRESS(ES) Naval Postgraduate School Monterey, CA 93943-5000	8. PERFORMING ORGANIZATION REPORT NUMBER
9. SPONSORING /MONITORING AGENCY NAME(S) AND ADDRESS(ES) N/A	10. SPONSORING/MONITORING AGENCY REPORT NUMBER

11. SUPPLEMENTARY NOTES The views expressed in this thesis are those of the author and do not reflect the official policy or position of the Department of Defense or the U.S. Government.

12a. DISTRIBUTION / AVAILABILITY STATEMENT Approved for public release; distribution is unlimited.	12b. DISTRIBUTION CODE

13. ABSTRACT (maximum 200 words)

This thesis presents the design and construction of a test-bed suitable for test and evaluation (T&E) of the Attitude Determination and Control System (ADCS) for a nanosatellite. This work briefly reviews the Navy's use of satellites and considers the role of nanosatellites within that context. A survey of three-axis simulators precedes the development of an adaptive mass-balancing algorithm capable of effectively eliminating gravitational torques on a three-axis simulator without momentum exchange devices. This is followed by the design and construction of a test-bed for validation of the mass-balancing algorithm.

Although primarily designed for integration within the NPS TINYSCOPE project, this test-bed's application reaches beyond TINYSCOPE to any payload onboard a nanosat requiring attitude control. The test-bed, based on the Cubesat standard, is modular and allows any ADCS, containable within a 1U (10 cm cube) space, to go through T&E prior to launch including, but not limited to, stability, pointing accuracy, and nadir tracking.

14. SUBJECT TERMS Spacecraft, Cubesat, Nanosat, Tinyscope, Simulator, Test Bed, Control, System Identification, Least Squares, Adaptive Mass Balancing, Mass Balancing, Three Axis Simulator, NACL, TAS, CubeTAS, ADCS	15. NUMBER OF PAGES 105
	16. PRICE CODE

17. SECURITY CLASSIFICATION OF REPORT	18. SECURITY CLASSIFICATION OF THIS PAGE	19. SECURITY CLASSIFICATION OF ABSTRACT	20. LIMITATION OF ABSTRACT
Unclassified	Unclassified	Unclassified	UU

NSN 7540-01-280-5500 Standard Form 298 (Rev. 8-98)
Prescribed by ANSI Std. Z39.18

THIS PAGE INTENTIONALLY LEFT BLANK

Approved for public release; distribution is unlimited

A THREE DEGREES OF FREEDOM TEST-BED FOR NANOSATELLITE AND CUBESAT ATTITUDE DYNAMICS, DETERMINATION, AND CONTROL

David M. Meissner
Lieutenant, United States Navy
B.S. Aerospace Engineering, United States Naval Academy, 2002

Submitted in partial fulfillment of the
requirements for the degree of

MASTER OF SCIENCE IN MECHANICAL ENGINEERING

from the

NAVAL POSTGRADUATE SCHOOL
December 2009

Author: David M. Meissner

Approved by: Marcello Romano
Thesis Advisor

Riccardo Bevilacqua
Co-Advisor

Knox Millsaps
Chairman, Department of Mechanical Engineering

THIS PAGE INTENTIONALLY LEFT BLANK

ABSTRACT

This thesis presents the design and construction of a test-bed suitable for test and evaluation (T&E) of the Attitude Determination and Control System (ADCS) for a nanosatellite. This work briefly reviews the Navy's use of satellites and considers the role of nanosatellites within that context. A survey of three-axis simulators precedes the development of an adaptive mass-balancing algorithm capable of effectively eliminating gravitational torques on a three-axis simulator without momentum exchange devices. This is followed by the design and construction of a test-bed for validation of the mass-balancing algorithm.

Although primarily designed for integration within the NPS TINYSCOPE project, this test-bed's application reaches beyond TINYSCOPE to any payload onboard a nanosat requiring attitude control. The test-bed, based on the Cubesat standard, is modular and allows any ADCS, containable within a 1U (10 cm cube) space, to go through T&E prior to launch including, but not limited to, stability, pointing accuracy, and nadir tracking.

THIS PAGE INTENTIONALLY LEFT BLANK

TABLE OF CONTENTS

I. INTRODUCTION 1
A. MOTIVATION: SURVEY OF THE NAVY'S USE OF SATELLITES 1
1. Communications 2
2. Intelligence 3
3. Positioning 3
4. Maritime Domain Awareness 3
B. LITERATURE REVIEW 6
1. Introduction 6
2. TINYSCOPE 9
3. State of the Art: A Survey of 3-Axis Simulators 10
a. Stanford 12
b. California State Polytechnic Institute (Cal Poly) 13
c. Virginia Polytechnic Institute and State University .. 14
d. Utah State University (USU) 15
e. Georgia Institute of Technology (GIT) 15
f. Naval Postgraduate School 16
C. THESIS OBJECTIVES 20
D. CONTRIBUTIONS 20

II. ANALYTICAL DEVELOPMENT 21
A. AUTOMATIC MASS BALANCING 21
B. PREVIOUS WORK AT NPS 22
1. System 22
2. Math 22
C. A NEW MASS BALANCING SYSTEM 23
1. System 23
2. Math 23
3. Simulation 26

III. ADCS TEST-BED DESIGN 33
A. INTRODUCTION 33
B. COMPONENTS 35
1. Structural 35
a. Spherical Air Bearing 35
b. Aluminum Support Structure 36
c. Air Bearing Mount 42
d. Bumper 42
e. Hemisphere 43
f. Polycarbonate Support 45
2. Electrical 46
a. Power 46
b. PC/104 47
c. Serial Board 48

d. A/D Board 48
e. Relay Board for Magnetic Control 48
3. Sensors 49
a. Inertial Measurement Unit 49
b. Inclinometers 51
c. Sun Sensor 52
d. Camera System 53
4. Actuators: Linear Motors 54

IV. CONCLUSION 65
A. SUMMARY OF WORK COMPLETED 65
B. CONTRIBUTIONS 65
C. LESSONS LEARNED 66

V. RECOMMENDATIONS FOR EXPERIMENTAL VALIDATION 67
A. GENERAL METHODOLOGY 67
B. SYSTEM IDENTIFICATION 67
C. RECOMMENDATIONS FOR FURTHER WORK 67

APPENDIX A: CUBESAT PARTICIPANTS LIST 69

APPENDIX B: PARTS 75

LIST OF REFERENCES 77

INITIAL DISTRIBUTION LIST 83

LIST OF FIGURES

Figure 1. ORBCOMM LEO Satellite [From 16] 5
Figure 2. CubeSat Specifications (From [19]) 7
Figure 3. Conception to Reality: Beanie Baby Box (left); Cubesat (right) 8
Figure 4. Poly Picosatellite Orbital Deployer(P-POD) (From [19]) 8
Figure 5. Tactical Imaging Nano-sat Yielding Small-Cost Operations and Persistent Earth-coverage (TINYSCOPE) (From [1]) 10
Figure 6. Air-Bearing Supported Platform Constructed at NASA Ames Research Center in 1959 (From [28]) 11
Figure 7. Three Standard Types of Spherical Air Bearing Systems 12
Figure 8. Orbiting Picosatellite Automated Launcher (OPAL) (From [30]) 13
Figure 9. The Cal Poly Spacecraft Dynamic Simulator (2007) 14
Figure 10. Virginia Tech Distributed Spacecraft Attitude Control System Simulator (DSACSS) (Whorl I, left; Whorl II, right) [From 27] 15
Figure 11. GIT Integrated Attitude Control System (IACS) (From [36]) 16
Figure 12. NPS Three-Axis Satellite Simulator (TASS) (From [37]) 17
Figure 13. NPS Three-Axis Simulator 2 (TAS2) (From [38]) 18
Figure 14. Automatic Mass Balancing System 21
Figure 15. Angular Momentum Error Transients 29
Figure 16. Center of Gravity Offset Transient 29
Figure 17. Angular Momentum 30
Figure 18. CG Offset 30
Figure 19. Center of Gravity Offset 31
Figure 20. Residual Torques 31
Figure 21. Cubesat Three-Axis Simulator (CubeTAS) 33
Figure 22. Aluminum Support Structure 34
Figure 23. CubeTAS Spherical Air Bearing (After [42]) 35
Figure 24. Pressure (psi) vs Lateral Position of various air bearings; From left to right: 1) Multiple orifices with no grooves, 2) Multiple orifices with distribution grooves, 3) Single orifice, no grooves, 4) Single non restrictive input port with depth and width of grooves providing restriction, 5) Full porous face with 10s of millions of sub-micron pores evenly spaced across the face (From [43]) 36
Figure 25. Aluminum Support Structure Preliminary Sketch 37
Figure 26. TECO Pneumatics, Inc., Draft of the Aluminum Support Structure (From [44]) 38
Figure 27. Structure: Version 1 39
Figure 28. Structure: Version 2 39
Figure 29. Structure: Version 3a 40
Figure 30. Structure: Version 3b 40
Figure 31. Structure: Version 4; Dimensions in inches 41
Figure 32. 80/20® Inc. 40-4040 Lite (From [45]); Dimensions in mm 42

Figure 33. Air-Bearing Mounting Plates; top view (left), side view (center), and bottom view (right) 42
Figure 34. Test-bed Protective Bumper 43
Figure 35. Teledyne Benthos 2040-10V Glass Sphere (From [45]) 43
Figure 36. CubeTAS Magnetic Coils 49
Figure 37. Analog Devices, Inc., ADIS16405/PCBZ (After [49]) 50
Figure 38. Rieker, Inc., N4 Inclinometer (From [50]) 51
Figure 39. SS-411 Two-Axis Digital Sun Sensor Mechanical Drawing (mm) (From [51]) 53
Figure 40. Potential Camera System for Angular Determination (After [53]) 54
Figure 41. New Scale Technologies, SQL-3.4-10 (From [54]) 54
Figure 42. Balance mass at maximum lateral position and elevation 57
Figure 43. Balance mass at minimum lateral position and elevation 58
Figure 44. Angle vs. Length 59
Figure 45. Angle vs. Length (0-30°) 59
Figure 46. Angle vs. Spring Constant 60
Figure 47. Angle vs. Spring Constant (0-30°) 60
Figure 48. Arm that Attaches Balance Masses to Squiggle Motor (dimensions are inches) 62
Figure 49. Stainless Steel Balance Masses with Attachment Arms 62

LIST OF TABLES

Table 1. AIS Data [From 14] 4
Table 2. Small Satellite Categorization Scheme [From 17, 18] 6
Table 3. Survey of Spacecraft Simulators; [1] California State Polytechnic University [25]; [2] Virginia Polytechnic Institute and State University [33]; [3] Utah State University [35]; [4] Naval Postgraduate School Three-Axis Spacecraft Simulator [37]; [5] Naval Postgraduate School Three-Axis Simulator Two [38]; [6] NASA Marshall Space Flight Center [39]; [7] Lawrence Livermore National Laboratory [33]; [8] Georgia Institute of Technology [36]; Naval Postgraduate School Cubesat Three-Axis Simulator 19
Table 4. Values Used in Simulation 27
Table 5. Spring Specifications 45
Table 6. Features of the Advanced Digital Logic ADLLX8PC–AMD Geode™ LX800 [After 47] 47
Table 7. Diamond-MM-32-AT [After 48] 48
Table 8. Analog Devices, Inc., ADIS16405/PCBZ Data [After 49] 50
Table 9. Rieker, Inc., N4 Inclinometer Data [After 50] 52
Table 10. SS-411 Two-Axis Digital Sun Sensor Data [After 51] 53
Table 11. SQL-3.4-10 Data [After 54] 55
Table 12. Spring Parameters for $\alpha = 25°$ 61

THIS PAGE INTENTIONALLY LEFT BLANK

LIST OF ACRONYMS AND ABBREVIATIONS

1U	1 Cubesat Volumetric Unit
2U	2 Cubesat Volumetric Units
3D	Three Dimensional
ACPI	Advanced Configuration and Power Interface
ACS	Attitude Control System
A/D	Analog to Digital
ADCS	Attitude Determination and Control System
AFRL	Air Force Research Laboratory
AIS	Automatic Information System
APM	Advance Power Management
CAD	Computer Aided Design
Cal Poly	California Polytechnic State University
CFR	Code of Federal Regulations
CG	Center of Gravity, equivalent to COM in a uniform gravitational field
CMG	Control Moment Gyroscope
CMR	Communications by Moon Relay
COM	Center of Mass, equivalent to CG in a uniform gravitational field
COR	Center of Rotation
COTS	Commercial-Off-The-Shelf
CP/SADS	Cal Poly Spacecraft Attitude Dynamics Simulator

CubeTAS	Cubesat Three-Axis Simulator
DC	Direct Current
DoD	Department of Defense
DSACSS	Distributed Spacecraft Attitude Control System Simulator
EIDE	Enhanced Intelligent Drive Electronics
EKF	Extended Kalman Filter
ETA	Estimated Time of Arrival
FAA	Federal Aviation Administration
FDM	Fused Deposition Modeling
Femtosat	Femto Satellite
FLTSATCOM	Fleet Satellite Communications
FOV	Field of View
GIT	Georgia Institute of Technology
GPS	Global Positioning System
GSFC	Goddard Space Flight Center
GT	Gross Tonnage
IACS	Integrated Attitude Control System
IMO	International Maritime Organization
IMU	Inertial Measurement Unit
I/O	Input/Output
ISIS	Innovative Solutions in Space
ITU	International Telecommunication Union
LEO	Low-Earth Orbit
LLNL	Lawrence Livermore National Laboratory

LOS	Line of Sight
M2M	Machine to Machine
MDA	Maritime Domain Awareness
MED	Momentum Exchange Device
Microsat	Micro Satellite
Minisat	Miniature Satellite
MMSI	Maritime Mobile Service Identity
MSFC	Marshall Space Flight Center
MUOS	Mobile User Objective System
NA	Not Applicable
NACL	Nanosat Advance Concepts Laboratory
Nanosat	Nano Satellite
NASA	National Aeronautics and Space Administration
NPS	Naval Postgraduate School
OD	Outer Diameter
OPAL	Orbiting Picosatellite Automated Launcher
OS	Operating System
PCB	Printed Circuit Board
Picosat	Pico Satellite
POC	Point of Contact
P-POD	Poly Picosatellite Orbital Deployer
RDTEN	Research, Development, Test and Evaluation, Navy
RTC	Real Time Clock
RW	Reaction Wheel

SATCOM	Satellite Communications
SDL	Space Dynamics Laboratory
Smallsat	Small Satellite
SOLAS	Safety of Life At Sea
SPI	Serial Peripheral Interface
SSACS	Small Satellite Attitude Control Simulator
SSBN	Nuclear Powered Ballistic Missile Submarine
SSD	Solid State Drive
SSIXS	Satellite Submarine Information Exchange Subsystem
SSN	Nuclear Powered Fast Attack Submarine
SSSL	Space Systems Simulation Laboratory
TAS2	Three-Axis Simulator 2
TASS	Three-Axis Spacecraft Simulator
TINYSCOPE	Tactical Imaging Nano-sat Yielding Small-Cost Operations and Persistent Earth-coverage
UFO	UHF Follow On
UHF	Ultra-High Frequency
USCG	United States Coast Guard
USN	United States Navy
USU	Utah State University
USW	Undersea Warfare
UTIAS/SFL	University of Toronto Institute for Aerospace Studies / Space Flight Laboratory
VT	Virginia Polytechnic Institute and State University

LIST OF VARIABLES

a	Major Axis Length (m)
α	Single Axis Elevation Angle (degrees)
$\mathbf{a}_b$	Sub-script denotes: Body Reference Frame
$\mathbf{a}'$	Prime denotes: Value or vector after offset compensation
b	Minor Axis Length
d_i	Balance Mass Deviation from Zero Location
$\Delta\mathbf{d}_i$	Balance Mass Displacement Vector
Δd_i	Scalar Balance Mass Displacement
e	Eccentricity
f	Flattening
F	Force (N)
$\mathbf{g}$	Gravity Vector
$\mathbf{H}$	Angular Momentum Vector
$\mathbf{H}_d$	Desired Angular Momentum Vector
$\mathbf{H}_{dd}$	Rate of Change of Desired Angular Momentum Vector
J	Inertia Matrix
$\hat{J}$	Estimate of the Inertia Matrix
$\hat{J}_s$	Estimate of the Inertia Matrix without Balance Masses
k	Scalar Gain or Spring Constant
K	Matrix Gain
m	Total Mass of the System (kg)
m_B	Total Mass of the Balance Masses

m_i	Individual Mass
O	Origin, COR
ϕ	Roll Angle
ψ	Yaw Angle
ρ_i	Zero Location of Each Balance Mass
r	Radius or Scalar Length of CG Offset Vector
r_{es}	Resolution
$\mathbf{r}$	Center of Gravity Offset Vector
$\hat{\mathbf{r}}$	Estimate of the Center of Gravity Offset Vector
$\mathbf{R}_O$	Center of Gravity Position Vector Without Balance Masses
$\mathbf{R}_i$	Location Vector of Each Balance Mass in the Spacecraft Body Frame, centered at O
t	Time or Thickness
θ	Pitch Angle
τ_a	Applied Torque
$\tau_{c\_\max}$	Maximum Attitude Control Torque
$\tau_{d\_\max}$	Maximum Planned on Orbit Torque
τ_g	Gravitational Torque
τ_r	Residual Torque
$\mathbf{u}_i$	Unit Vector in the Direction of Travel of a Balance Mass
$\mathbf{u}_s$	Stabilizing Command
ω	Angular Velocity (rad/sec)

ACKNOWLEDGMENTS

I would like to thank my God for giving me the strength and wisdom required over the past year to complete this project. Many thanks to my wife, Tracy, for her constant support and encouragement, and an occasional swift kick in the pants required to revitalize my motivation on the longest days and nights. I would also like to thank Claudia and Larry Calahan for their help in editing this document.

I would like to acknowledge the work of my co-advisors, Dr. Romano and Dr. Bevilacqua, for their countless hours of help with mathematical calculations, modeling, and guidance over the past year. In addition, Dr. Hyunwook's work has been invaluable. Thanks to Dr. Jae Jun Kim for his assistance and guidance throughout the project. Many thanks to their work, and those of: MAJ Chad Melone, MAJ Chris Ortiona, LCDR Jason Hall, Paul Oppenheimer, LT Jason Tuthill and Karl Gramespacher.

Thanks to John Mobley and Glenn Harrell for all the machining required and to Donna Cuadrez for all her help in the editing process. Thank you, LT Doug Smith, for carrying on with this project. Godspeed!

THIS PAGE INTENTIONALLY LEFT BLANK

I. INTRODUCTION

A. MOTIVATION: SURVEY OF THE NAVY'S USE OF SATELLITES

This thesis intends to support the Naval Postgraduate School (NPS) Cubesat program and potential advances in USW intelligence gathering capabilities by contributing to the design and construction of a Cubesat Three-Axis Simulator for NPS termed CubeTAS. This thesis also documents the design and development of CubeTAS.

The capabilities of a constellation of cubesats can provide real time space-based observation of ports with tactically relevant revisit times [1]. The first section of the introduction aims to present a few areas in which Cubesats may serve the Navy more aptly and more cheaply than current space systems.

This test-bed is intended for immediate implementation in support of the Naval Postgraduate School's TINYSCOPE nanosat program with additional testing of passive magnetic control within the NPS Small Satellite Research Lab's Helmholtz coil. The simulator will then be available for other Nanosats within the academic community to provide a practical and affordable test bed for continued education in space, space systems, and relevant military applications.

The primary purpose of this test bed is to allow for nanosat attitude determination and control system (ADCS) development, sensor integration for pre-flight tests, and precision pointing algorithm validation. The secondary purpose of this work is verification of hardware in the loop, which would allow for performance verification of momentum exchange devices (MEDs) in the form of passive magnetic control, reaction wheels, or active control moment gyroscopes (CMGs).

In order to provide a torque-free simulator, a test bed must be designed and constructed in such a way that the center of gravity (CG) and center of rotation (COR) are co-located. Although course and fine resolution techniques

can be used to approach this end manually, fine resolution is only attained through the real time implementation of adaptive mass-balancing onboard the simulator.

1. Communications

The Navy began developing satellite communication with the installation of mobile terminals on USS Midway (CVA-41) and USS Canberra (CAG-2) in 1965 [2]. Satellite relay from shore stations has been a very effective means of conveying orders and critical information to ships, submarines, and aircraft at sea. The year 1958 saw the dawn of satellite communications in the form of Communications by Moon Relay (CMR), followed by the first man-made passive reflector called Echo, which was launched by NASA in August 1960 [3, pp. 38–40]. The Telstar program, an effort mainly of AT&T, followed Echo and demonstrated that "active communication satellites could provide high-quality stable circuits for television and multi-channel telephony" [4, pp. 3–5]. Since 1976, the Navy has relied on ultra-high frequency (UHF) Satellite Communications (SATCOM) [5].

Satellites currently disseminate information to Attack Submarines (SSN) and Ballistic Missile Submarines (SSBN) via the Satellite Submarine Information Exchange Subsystem (SSIXS). This system transmits data to its subscribers, who can receive group broadcasts or request message traffic waiting in a queue. Fleet Satellite Communications (FLTSATCOM) satellites were the first to provide this capability with coverage between 70 degrees North and 70 degrees South latitude [6]. FLTSATCOM satellites where replaced by UHF Follow On (UFO) satellites in the 1990s. The UFO satellites are being updated and scheduled for replacement by the Mobile User Objective System (MUOS) beginning in 2010 with MUOS attaining full capability in 2014 [7, 8]. All of these systems provide for select information to be transmitted to submarines underway with near global coverage.

2. Intelligence

Satellites have been used since August 1960 to make photo reconnaissance observations from space starting with the launch of the Corona spacecraft [9]. Nations have used satellites to observe foreign ports, to track submarine in-port time and deployment schedules. These observations give our forces a more accurate depiction of enemy positions and capabilities and allows the Unites States to appropriately allot funding to critical force structure to maintain sufficient strategic, operational, and tactical advantage over our adversaries.

3. Positioning

The Global Postioning System (GPS) has had an invaluable influence on navigation, and revolutionized positioning data for accurate weapon systems launch parameters. For submarines in particular, celestially based measurements of the Earth's gravity field are used to create vertical deflection maps, which, in turn, provide compensation for gyroscopic errors [10].

4. Maritime Domain Awareness

Maritime Domain Awareness (MDA) is the Navy's way of collecting tracking data on vessels at sea the same way the Federal Aviation Administration (FAA) keeps track of aircraft. The Navy uses a system called the Automatic Information System (AIS) to collect and organize the data. The U.S. Coast Guard (USCG) became very interested in the program shortly after the attacks on New York in 2001 [11].

The Automatic Information System is a network of transponders that the International Maritime Organization's (IMO) International Convention for the Safety of Life at Sea (SOLAS) requires onboard ships with a gross tonnage (GT) of 300 or more tons and all passenger ships [12]. The Code of Federal Regulations Title 70 Part 80.5 provides the official definition of AIS as:

> A maritime navigation safety communications system standardized by the International Telecommunication Union (ITU) and adopted by the International Maritime Organization (IMO) that provides vessel information, including the vessel's identity, type, position, course, speed, navigational status and other safety-related information automatically to appropriately equipped shore stations, other ships, and aircraft; receives automatically such information from similarly fitted ships; monitors and tracks ships; and exchanges data with shore-based facilities. [13]

These transponders mainly operate within the VHF band and are restricted to Line-of-Sight (LOS) transmission. Although there are 26 different message types, the representative data shown in Table 1 is transmitted via AIS [12,14].

Every 2 to 10 seconds while underway and every 3 minutes at anchor	**Every 6 minutes**
Maritime Mobile Service Identity (MMSI)	IMO Ship Identification Number
Navigation Status	Radio Call Sign
Rate of Turn	Vessel Name
Speed Over Ground	Type of Ship and Cargo
Position Accuracy	Ship Dimensions
Course Over Ground	GPS Antenna Location
True Heading	Type of Positioning Data
Time Stamp	Ship Draught
	Destination
	Estimated Time of Arrival (ETA)

Table 1. AIS Data [From 14]

ORBCOMM is currently the provider of AIS data to the USCG and U.S. Navy (USN). ORBCOMM is a civilian organization aimed at Machine-to-Machine (M2M) two-way data communication between fixed or mobile assets such as

commercial transportation, heavy equipment, industrial fixed assets, and marine/homeland security assets [15].

ORBCOMM's current satellites, depicted in Figure 1, exist in Low-Earth Orbit (LEO) and utilize a wheel-augmented gravity gradient/magnetic 3-axis Attitude Control System (ACS). They do not require a propulsion system for station keeping, but the base subsystem advertises "cold gas propellant / differential drag station keeping" [16].

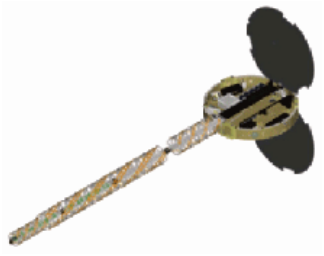

Figure 1. ORBCOMM LEO Satellite [From 16]

ORBCOMM currently has AIS data collection systems onboard five of their satellites with plans to launch 18 more with increased processing power of the same data by the start of 2011 [11]. ORBCOMM is also considering a polar orbiter allowing AIS data to be collected throughout the globe, and routed to select terrestrial ground stations via onboard "store and forward". AIS data, on vessels up to 72 degrees latitude, is currently available to subscribers via the World Wide Web and other data networks [11].

Cubesats at NPS are being developed for their utility in photo reconnaissance. Constellations of cubesats could soon be utilized as communications relays for time critical orders, sensors gathering earth science data for civil or military applications, or as a Department of Defense (DoD) supplement to the current AIS framework.

B. LITERATURE REVIEW

1. Introduction

Commercial satellites tend to have a wet mass, which includes fuel, in the range of 1000–4000 kg (2200–8800 lbm). In order to make satellites faster, better, smaller, and cheaper, research has been conducted over the past 20–30 years to develop smaller satellites. Smallsats (< 500 kg) tend toward the use of Commercial-Off-The-Shelf (COTS) equipment as opposed to organic components, and they have shorter kick-off to launch times with subsequently lower overall costs. Within the realm of Smallsats, the generally accepted classification scheme, based on wet mass, is shown in Table 2.

Group Name	Wet Mass	
Large Satellite	> 1000 kg (> 2200 lbm)	
Medium Sized Satellite	500–1000 kg (1100–2200 lbm)	
Mini Satellite (Minisat)	100–500 kg (220–1100 lbm)	Small Satellites (Smallsats)
Micro Satellite (Microsat)	10–100 kg (22–220 lbm)	
Nano Satellite (Nanosat)	1–10 kg (2.2–22 lbm)	
Pico Satellite (Picosat)	0.1–1 kg (0.22–2.2 lbm)	
Femto Satellite (Femtosat)	<100 g (<0.22 lbm)	

Table 2. Small Satellite Categorization Scheme (From [17, 18])

Smallsats are of particular interest to the DoD due to their lower cost and the short conception to launch time requirements allowing the military to deliver a fast turn-around on short-term missions. According to the NASA Goddard Space Flight Center (GSFC), in the next one to eight years, smallsats will become more common as components are miniaturized as a by-product of advances in industry [17]. There will always be a place for a wide range of satellites across the spectrum of possible masses, but smallsats are very quickly finding their niche.

Cubesats, with a mass of 1 kg, are technically picosatellites that have been designed or built to the Cubesat standard, Figure 2, as designed by Stanford and the California Polytechnic State University (Cal Poly) [19]. These smallsats have a nominal construction cost of $30,000–$40,000 and a launch cost of $40,000 [20]. Cubesat kits can be purchases from Pumpkin, Inc., starting with a Cubesat skeleton for $7,500 [21]. Cubesats can be built and launched within a year [22]. A list of groups working on Cubesats is included as Appendix A.

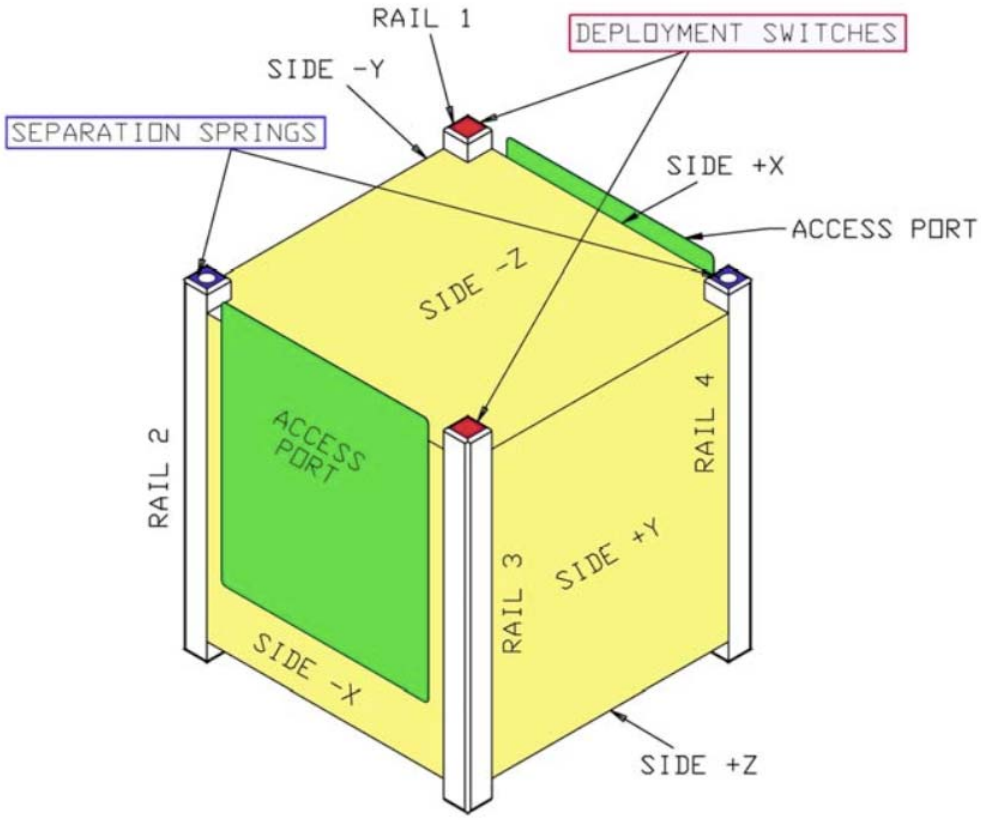

Figure 2. CubeSat Specifications (From [19])

Based originally on a Beanie Baby box, the standard unit of a Cubesat, such as CP-1 shown in Figure 3, is a 10 cm cube, termed 1 Unit or 1U. Cubesats can range from 1U up to any combination that can be designed and launched, e.g., 2U (10x20 cm) or 3U (10x30 cm).

Figure 3. Conception to Reality: Beanie Baby Box (left); Cubesat (right)

Cal Poly has designed a tube-type spring loaded Cubesat launcher, shown in Figure 4, called the Poly Picosatellite Orbital Deployer, or P-POD, capable of launching any combination of 1U, 2U and 3U Cubesats taking no more than a 3U volume. Other groups, e.g., ISIS, UTIAS/SFL, also provide launch capability.

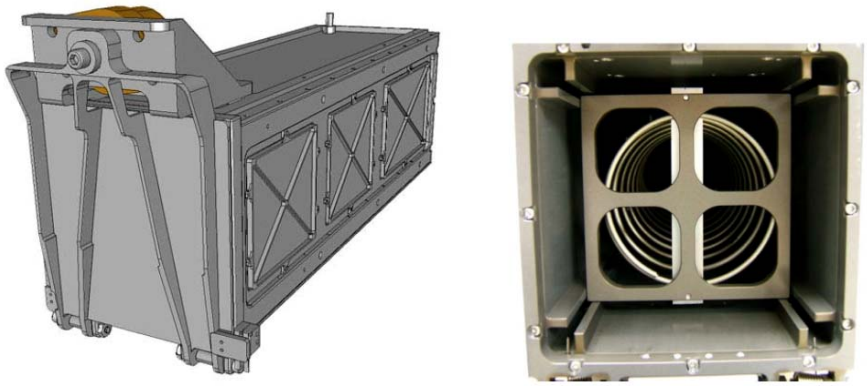

Figure 4. Poly Picosatellite Orbital Deployer(P-POD) (From [19])

Cal Poly's Professor Jordi Puig-Suari took the initiative to start an annual Cubesat Developers' Workshop in April 2004, which now serves as an "international collaboration of over 40 universities, high schools, and private firms developing picosatellites containing scientific, private, and government payloads" [18].

Smallsats have the ability to change the way the DoD thinks about accomplishing missions in space. With a constellation of 80 nanosatellites, revisit time can be reduced down to less than 30 minutes. [1, p.10]. A geo-

stationary orbit overhead a target of interest would be optimal giving maximum overhead time, but these orbits can only reside along the Earth's equator. And these orbits, which are positioned around 35,800 km above the earth, do not lend themselves to high-resolution imagery. The best altitude for quality images is the Low Earth Orbit (LEO), which is nominally defined as less than 2000 km. A LEO Sun-synchronous polar orbit, or polar orbit, allows the Earth to rotate underneath the satellite's orbit which can allow for full earth coverage provided specific combinations of altitude and sensor swath width are met. Orbits can be adjusted to get twice daily coverage of any location on the globe from any one satellite [23].

2. TINYSCOPE

Tactical Imaging Nano-sat Yielding Small-Cost Operations and Persistent Earth-coverage (TINYSCOPE), shown in Figure 5, is a cubesat design at NPS being designed to provide real time intelligence to operational and tactical level forces in theatres like Iraq and Afghanistan [1]. A student at NPS conducted an analytical feasibility study to develop estimates of potential performance and tactical usefulness of the TINYSCOPE concept. A constellation of nanosats, like TINYSCOPE, would be capable of the tactically relevant revisit times as mentioned above [1].

Figure 5. Tactical Imaging Nano-sat Yielding Small-Cost Operations and Persistent Earth-coverage (TINYSCOPE) (From [1])

3. State of the Art: A Survey of 3-Axis Simulators

The Attitude Determination and Control System (ADCS) is the subsystem in charge of estimating and controlling the orientation of the satellite. There are a variety of methods available for use as ADCS systems. In terms of sensing, sensors have been developed that measure satellite attitude with respect to the stars, termed Star Trackers. A similar sensor, which looks at only one star, our sun, is termed a Solar Tracker. The list goes on to include horizon sensors, orbital gyrocompasses, and magnetometers [24]. The attitude determination is usually performed fusing the sensors' measurements via a digital extended Kalman Filter [25].

There are two main categories of attitude control: passive and active. Passive control can consist of gravity gradient stabilization, which uses satellite asymmetry to align the long axis of the satellite with the center of the Earth, or

the more complex magnetic torquers, which use permanent magnets, or coils, and a precise map of the Earth's magnetic field to control rotation [26].

Active control, the traditional form of attitude control, can take the form of thrusters expending propellant, spin stabilization, solar sails, or Momentum Exchange Devices (MED), e.g., Reaction Wheels (RW) or Control Moment Gyroscopes (CMG) [26].

In order to test ADCS algorithms on the ground, prior to launch, simulation of dynamics within a test-bed allows researchers to adequately model the system as it would exist in the space environment and run tests on the space vehicle's attitude determination and control system.

Three-axis simulators are common within the Aerospace industry and education system. Three-axis simulators for cubesats are less common and, in fact, this thesis aims to be the first. One of the first attitude simulators, shown in Figure 6, was built at the NASA Ames Research Center in 1959 [28, p. 3].

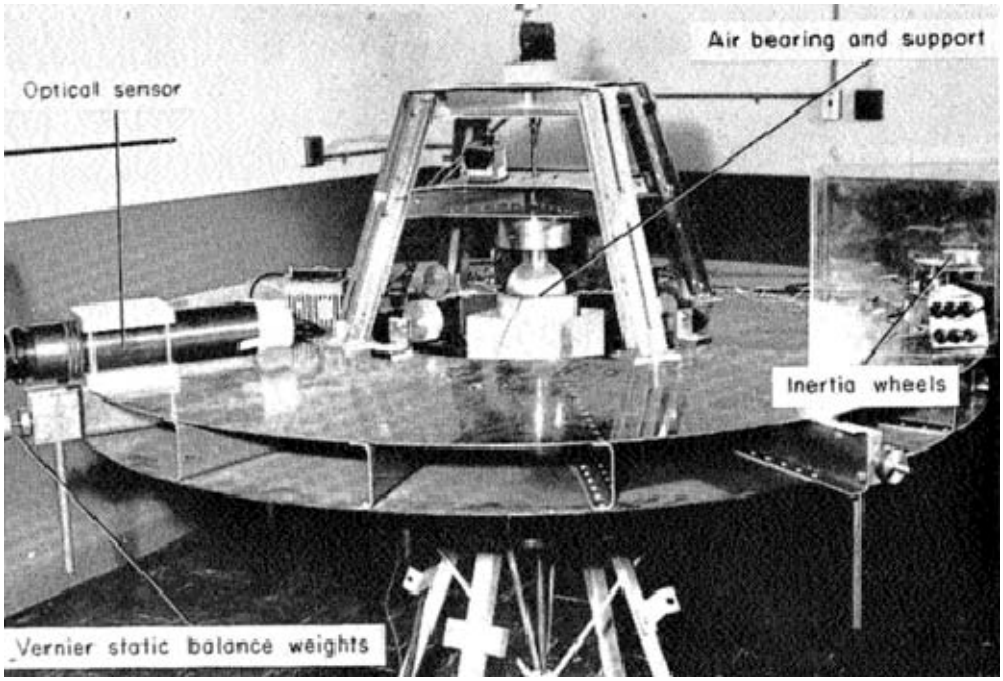

Figure 6. Air-Bearing Supported Platform Constructed at NASA Ames Research Center in 1959 (From [28])

Schwartz, Peck and Hall wrote a historical review of air-bearing spacecraft simulators in 2003. They looked at planar systems, rotational air-bearings and facilities that had the capability to provide translational and three-dimensional rotational freedom [28]. In terms of rotational systems, as the one being developed here, there are three basic types of spherical air bearing platforms: tabletop (Figure 7a), umbrella (Figure 7b) and dumbbell (Figure 7c).

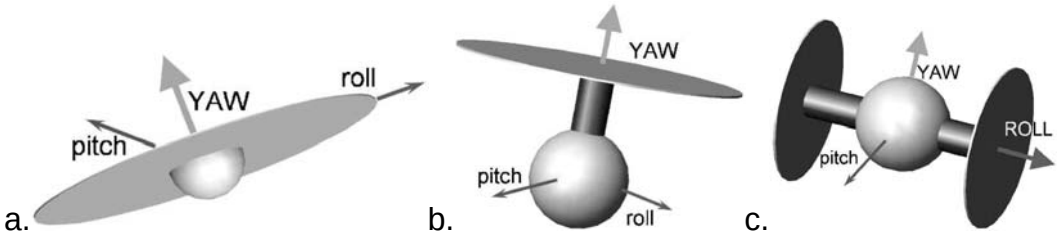

Figure 7. Three Standard Types of Spherical Air Bearing Systems

The tabletop design has the system components mounted on top of the "table." The umbrella is designed to keep the center of mass of the system very near to the center of rotation by suspending components very carefully below the "umbrella." The dumbbell design reduces structural interference by placing the payload of the simulator further from the center of rotation [28, p. 515]. A set of three or four gimbals, four to avoid gimbal lock, can be used instead of a spherical air bearing, but it has been determined that gimbal dynamics will interfere with the dynamics of the payload as a non-linear function of the gimbal angle creating increased complexity [28, p. 513].

a. Stanford

The first unclassified/non-proprietary spherical air-bearing simulator was built at Stanford around 1975 [28, p. 516]. In 1996, Professor Robert Twiggs advised Jaewoo Jung, Naoki Kuzuya and Jaime Alvarez on the design of the Orbiting Picosatellite Automated Launcher (OPAL) attitude control system using two pairs of magnetic coils and a 3-axis magnetometer. Ground simulations of the ADCS for OPAL (Figure 8) were run, using a computer model [29].

Figure 8. Orbiting Picosatellite Automated Launcher (OPAL) (From [30])

b. California State Polytechnic Institute (Cal Poly)

The Cal Poly Spacecraft Attitude Dynamic Simulator (CP/SADS), as of August 2007, was set up with four reaction wheel momentum exchange devices in a pyramid configuration mounted on a spherical air bearing [31, p. 1]. Figure 9 shows the August 2007 design configuration, which was designed to weigh less than 10 kg [31, p. 5]. The CP/SADS is capable of $360°$ of rotation about the z-axis and $\pm 30°$ about the x-axis and y-axis, with 0.1 rad/s and 0.1 rad/s^2 angular velocity and acceleration, respectively [31, p. 4]. Test results showed that CP/SADS has a pointing accuracy of around $2-3°$ [31, p. 22].

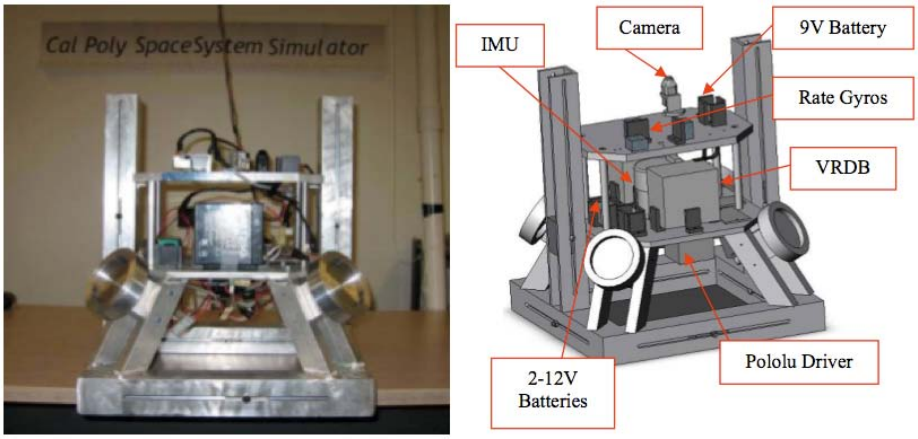

Figure 9. The Cal Poly Spacecraft Dynamic Simulator (2007)

In 2007, Cal Poly's team was moving toward a mass estimation scheme published by Tanygin and Williams [31]. Healy ran a computer simulation of the system identification and automatic mass balancing of CP/SADS using a least squares technique [31]. Mehiel and Silva are in the progress of publishing a thesis documenting the implementation of Healy's theoretical work [32]. CP/SADS was sponsored by the Department of the Navy, Office of Naval Research, under Award # N00014-05-1-0855 [31, p. 23].

c. Virginia Polytechnic Institute and State University

The Space Systems Simulation Laboratory (SSSL) at Virginia Tech currently has a Distributed Spacecraft Attitude Control System Simulator (DSACSS), Figure 10. DSACSS is "two independent spherical air-bearing platforms for formation flying attitude control simulation" [33]. Virginia Tech is working on energy storage techniques and control options that include coupled attitude control and nonlinear compensation of an under-actuated system [33]. DSACSS is also being used for magnetic bearing research and work on attitude control via combinations of control moment gyros, momentum wheels, and thrusters. See Table 3 for a summary of Virginia Tech's DSACSS capabilities.

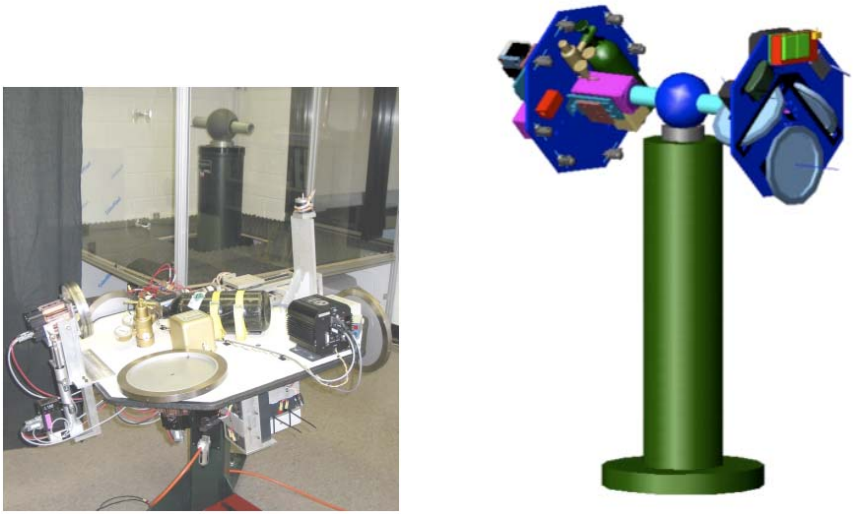

Figure 10. Virginia Tech Distributed Spacecraft Attitude Control System Simulator (DSACSS) (Whorl I, left; Whorl II, right) [From 27]

Virginia Tech's work is supported by: the Air Force Research Lab (AFRL), Air Force Office of Scientific Research, Honeywell Aerospace, the National Aeronautics and Space Administration, and the National Science Foundation [33].

d. Utah State University (USU)

According to [34], Utah State developed a test bed named the Small Satellite Attitude Control Simulator (SSACS) in the 1990s with an adaptive mass balancing system as detailed in theses by Young and Olson.

USU is planning on revealing a very capable laboratory for cubesats in the near future. Although, this author is not at liberty to divulge the details of USU's Space Dynamics Laboratory (SDL), this lab will provide great opportunities for cubesat research [35]

e. Georgia Institute of Technology (GIT)

As of 2003, Georgia Tech had developed an Integrated Attitude Control System (IACS) with a 136 kg (300 lbf) load capacity, four CMGs, and

pneumatic thrusters in addition to the attitude and rate sensors [36]. The IACS is shown in Figure 11, and other comparison data is shown in Table 3.

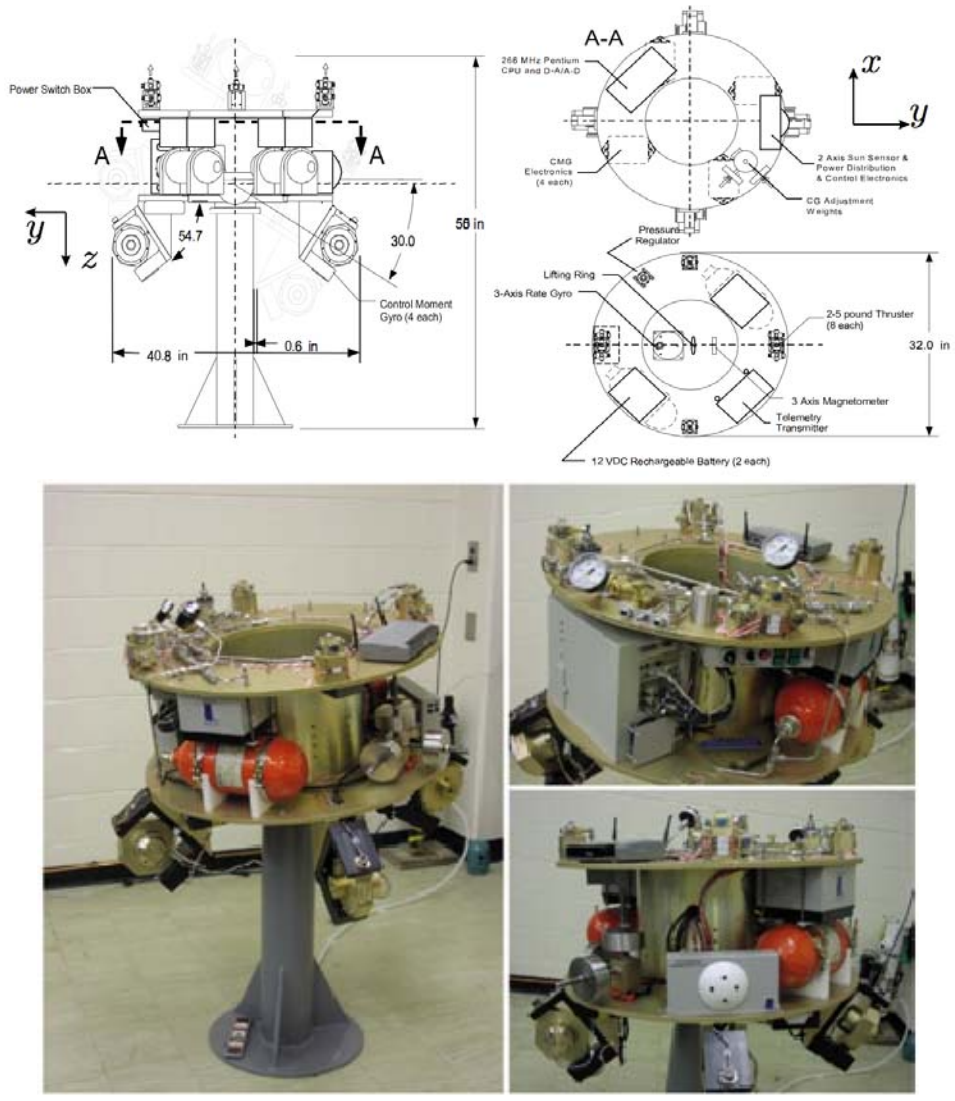

Figure 11. GIT Integrated Attitude Control System (IACS) (From [36])

f. Naval Postgraduate School

The Naval Postgraduate School has developed state-of-the-art satellite simulators. Two representative test beds have been chosen for presentation here: the Three-Axis Spacecraft Simulator (TASS) (Figure 12) and the Three-Axis Simulator 2 (TAS2) (Figure 13) [37, 38]. Generic capability numbers are included in Table 3, and further information can be found in [37, 38].

CubeTAS aims to be the fourth spacecraft simulator at NPS with the following capabilities/sensors:

- 2 single-axis inclinometers
- Inertial Measurement Unit
- Sun Sensor with externally simulated light source
- One single-axis reaction wheel for active attitude control
- Helmholtz Coil for magnetic field simulation
- Torque Coils for passive attitude control
- Modular 1U volume for further research

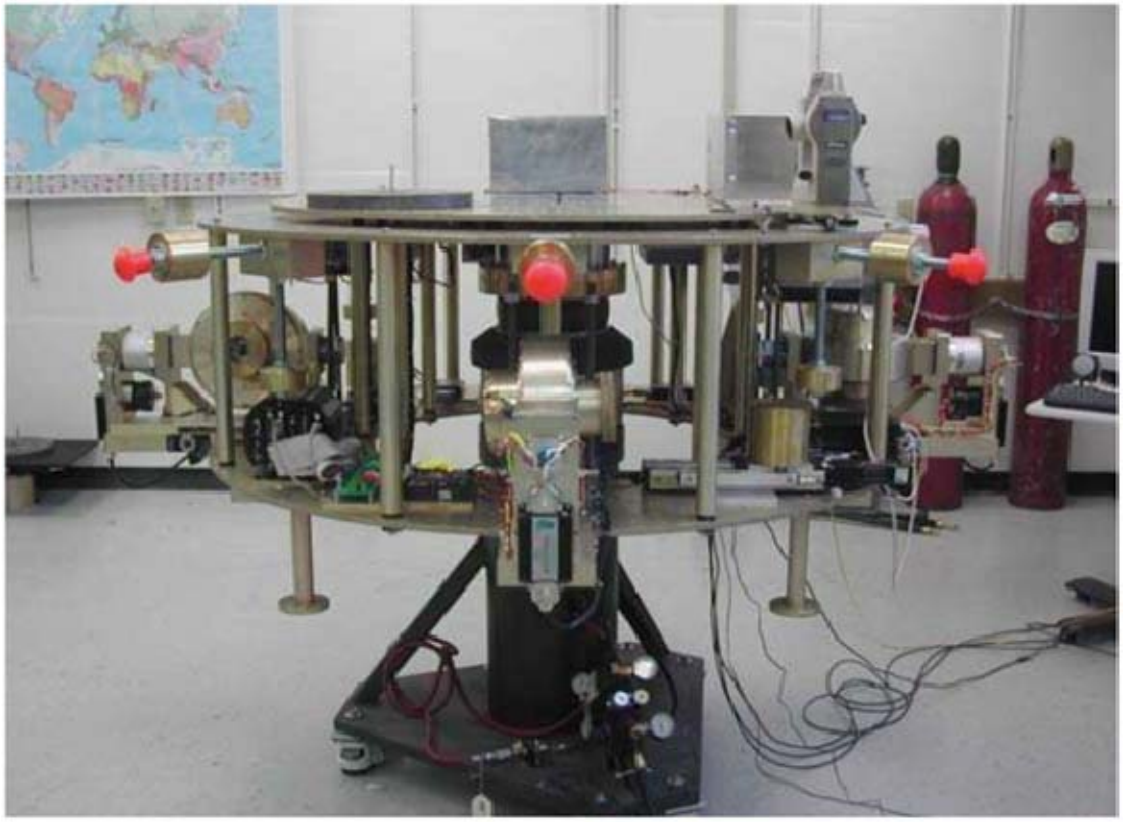

Figure 12. NPS Three-Axis Satellite Simulator (TASS) (From [37])

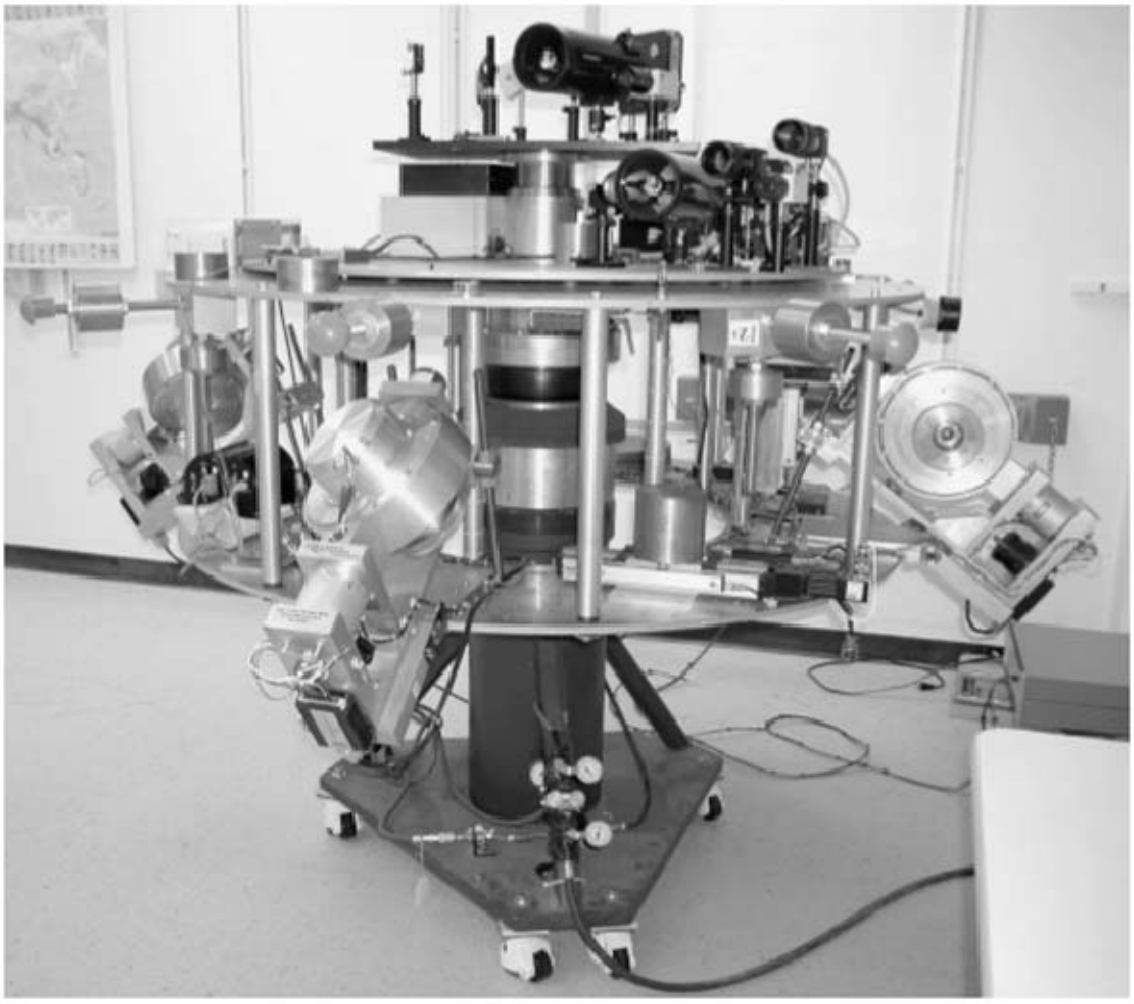

Figure 13. NPS Three-Axis Simulator 2 (TAS2) (From [38])

Table 3 provides a broad overview of a wide range of spacecraft simulators from the university level to world-class work being done by the National Aeronautics and Space Administration.

Facility	DoF	Yaw	Pitch	Roll	Weight	CMG	RW	Thrusters	Pointing Accuracy	Auto Mass Balancing
Cal Poly[1]	3	360°	± 30°	± 30°	10 kg (22 lb)	No	Yes	No	2-3°	In works
VT[2]	3	360°	a: ± 5° b: ± 30°	a: ± 5° b: ± 30°	136 kg (300lb)	Yes	Yes	Yes	TBD	Yes
USU[3]	Very Capable System In Works									
NPS TASS[4]	3	360°	± 30°	± 30°	200 kg (441 lb)	No	Yes	No	0.1°	Yes
NPS TAS2[5]	3	360°	± 20°	± 20°	800 kg (1763 lb)	Yes	No	No	<0.1°	Yes
MSFC[6]	6	360°	360°	360°	181kg (400 lb)					
LLNL[7]	4	360°	± 15°	± 30°	32 kg (70 lb)					
GIT[8]	3	360°	± 30°	± 30°	136 kg (300 lbf)	Yes	Yes	Yes	<1°	Yes
NPS CubeTAS[9]	3	360°	± TBD°	± TBD°	8 kg (18 lb)	No	Yes	No	TBD	In works

Table 3. Survey of Spacecraft Simulators; [1] California State Polytechnic University [25]; [2] Virginia Polytechnic Institute and State University [33]; [3] Utah State University [35]; [4] Naval Postgraduate School Three-Axis Spacecraft Simulator [37]; [5] Naval Postgraduate School Three-Axis Simulator Two [38]; [6] NASA Marshall Space Flight Center [39]; [7] Lawrence Livermore National Laboratory [33]; [8] Georgia Institute of Technology [36]; Naval Postgraduate School Cubesat Three-Axis Simulator

C. THESIS OBJECTIVES

After the survey of this chapter, it was determined that the CubeTAS will be the first three-axis simulator specifically designed to accommodate the cubesat form factor and constitutes a new, spherical, air-bearing design unlike those shown in Figure 7. This design type has been termed, by the author, a "bowl" type spherical air-bearing test-bed. This thesis introduces a new mass balancing technique not involving momentum exchange devices for angular momentum inputs. Only the balance masses themselves will be manipulated in order to collocate the system's center of gravity and center of rotation. This mass-balancing algorithm is to be validated by the design and construction of a three-axis simulator.

Chapter II will follow the analytical derivation of the CubeTAS adaptive mass-balancing algorithm. Chapter III includes a discussion of the CubeTAS design to include drawings and component specifications. Chapter IV contains the summary and conclusion, and Chapter V covers future experimental validation and recommendations for further work.

D. CONTRIBUTIONS

In term of the goals of this thesis, the CubeTAS project sought to make the following contributions:

- Design of Three-Axis Simulator with the aid of CAD programs and a 3D printing machine
- Test-bed for Nanosatellite attitude dynamics testing
- A new mass-balancing technique
- Construction of the test-bed for simulation validation

II. ANALYTICAL DEVELOPMENT

A. AUTOMATIC MASS BALANCING

A standard configuration for an automatic mass-balancing system is comprised of three independently controlled masses designed to move parallel to each of the three principle axes of the system. The following derivations are based on those demonstrated in [34]. Figure 14 shows the generic layout, where ρ_i denotes the zero location of each balance mass and d_i denotes deviation from the zero location. The unit vector along which each mass, m_i, travels is represented as u_i.

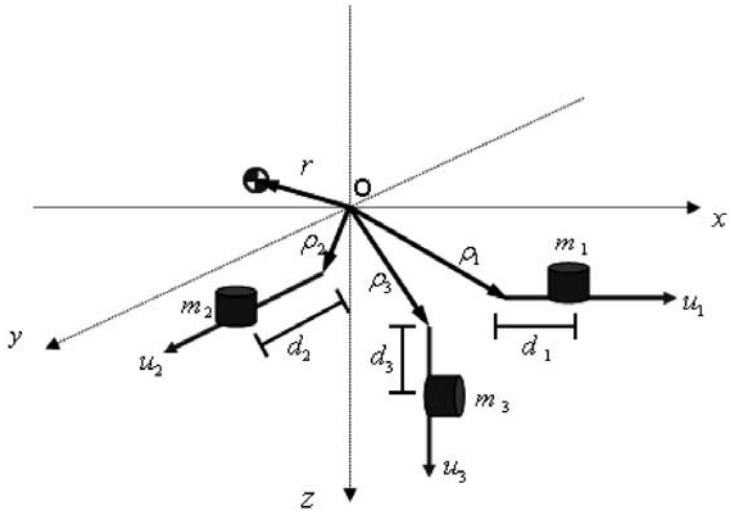

Figure 14. Automatic Mass Balancing System

If the center of gravity (CG) is located at the tip of the position vector, $\mathbf{r}$, the balance mass positions are manipulated to reduce $|\mathbf{r}|$ as closely as possible to zero, where O denotes both the origin of the spacecraft inertial body frame and the center of rotation (COR) of the simulator. The length of $\mathbf{r}$ is often reduced by manual manipulation of masses external to the system shown in Figure 14. This brings $|\mathbf{r}|$ into a range of controllability based on m_1, m_2, m_3 and the range of travel of the balance masses.

The location of each balance mass can be denoted

$$\mathbf{R}_i = \boldsymbol{\rho}_i + d_i \mathbf{u}_i \qquad (i = 1...3) \tag{1}$$

Following [34] the CG vector is then calculated as

$$\mathbf{r} = \frac{1}{m}\int_B R\, dm = \frac{1}{m}\left[(m - m_B)\mathbf{R}_O + \sum_{i=1}^{3} m_i \mathbf{R}_i \right] \tag{2}$$

where $m_B = m_1 + m_2 + m_3$ is the sum of the balance masses, $\mathbf{R}_O$ is the CG vector without balance masses and m is the total mass of the entire system.

B. PREVIOUS WORK AT NPS

1. System

The 3-axis spacecraft simulators at NPS use an umbrella type spherical air bearing. They are nominally of significant mass and the increased volume available has provided researchers greater flexibility allowing the use of momentum exchange devices on each axis for integration in the mass-balancing algorithm. This allows the simulators to be continually perturbed preventing the case where the CG may be improperly placed below the COR.

2. Math

The change in balance mass displacement, Δd, can be written in general terms as

$$\Delta \mathbf{d} = -\begin{bmatrix} \frac{m}{m_1} r_1 & \frac{m}{m_2} r_2 & \frac{m}{m_3} r_3 \end{bmatrix}^T \tag{3}$$

where $\hat{\mathbf{r}}$ is the estimate of the CG vector including the balance masses. It can also be shown that the estimated inertia matrix, $\hat{J}$, can be broken up into two terms, the estimate without balance masses, $\hat{J}_s$, and the inertia of the balance masses alone. This estimate can be written as

$$\hat{J} = \hat{J}_s + \sum_{i=1}^{3} (-m_i [\mathbf{R}_i \times][\mathbf{R}_i \times]) \tag{4}$$

where $[\mathbf{R}_i\times]$ represents the cross product matrix of the $i\text{th}$ balance mass with the cross product matrix defined as

$$[\mathbf{a}\times]=\begin{bmatrix} 0 & -a_3 & a_2 \\ a_3 & 0 & -a_1 \\ -a_2 & a_1 & 0 \end{bmatrix}, \quad \mathbf{a}=\begin{bmatrix} a_1 \\ a_2 \\ a_3 \end{bmatrix} \tag{5}$$

The new inertia matrix estimate after CG offset compensation is found by subtracting the initial contribution of the balance masses to the inertia matrix and replacing it with the updated estimate, where the new estimate becomes

$$\hat{J}' = \hat{J} - \sum_{i=1}^{3}(-m_i[\mathbf{R}_i\times][\mathbf{R}_i\times]) + \sum_{i=1}^{3}(-m_i[\mathbf{R}_i'\times][\mathbf{R}_i'\times]) \tag{6}$$

The first step in Kim and Agrawal's method is batch estimation of the inertia matrix and the center of gravity. The control method used involves adaptation and continuous excitation with a "preplanned spacecraft momentum trajectory" [34]. The error value between the actual and this desired angular momentum is decreased toward zero. At this point gravitational disturbances are eliminated. Kim and Agrawal use momentum exchange devices to follow the desired angular momentum trajectory.

C. A NEW MASS BALANCING SYSTEM

1. System

With the aim of developing a method for gravitational torque cancellation without momentum exchange devices, the CubeTAS was constructed without momentum exchange devices. These components can be added, if desired, into the modular 1U space in the center of the simulator but are not critical to the performance of the mass-balancing algorithm.

2. Math

The following analysis is a preliminary analytical development meant to prelude the introduction of the mass-balancing algorithm to the CubeTAS. Most of this development follows very closely the work of Kim and Agrawal, [34], with

minor variations made to remove MED requirements from the system. Instead of MEDs, the masses themselves are used to generate the torques required to balance the system, i.e., reduce the norm of the CG offset vector toward zero.

The author's approach incorporates the adaptation law from [34] but sums this term with another based on the removal of MEDs from the system. In this manner the term $\delta\mathbf{r}$, which represents the change of the CG due to automatic mass balancing actuation, is broken into two parts, which can be written

$$\delta\mathbf{r} = \delta\mathbf{r}_1 + \delta\mathbf{r}_2 \tag{7}$$

where $\delta\mathbf{r}_1$ represents the same changes in CG referred to in [34], and $\delta\mathbf{r}_2$ represents those changes in CG required without the use of MEDs. What follows is a brief explanation of the control method developed for CubeTAS.

As mentioned above, the simulator must be excited by an angular momentum input around each axis to avoid the case in which the CG settles along the gravity vector. A desired trajectory, $\mathbf{H}_d$, is generated based on the Lyapunov function

$$V(\mathbf{H}, \delta\mathbf{r}_1) = \frac{1}{2}(\mathbf{H} - \mathbf{H}_d)^T(\mathbf{H} - \mathbf{H}_d) + \frac{1}{2}(\mathbf{r}_0 + \delta\mathbf{r}_1)^T \Gamma^{-1}(\mathbf{r}_0 + \delta\mathbf{r}_1) \tag{8}$$

where $\mathbf{H}$ is the current angular momentum of the simulator, $\mathbf{H}_d$ is the desired angular momentum trajectory, $\mathbf{r}_0$ is the CG location at time zero, $\delta\mathbf{r}_1$ is the change of the CG due to automatic mass-balancing actuation, and Γ is a symmetric positive definite matrix.

It can be shown, that the rate of change of the CG vector can be represented as

$$\delta\dot{\mathbf{r}}_1 = m\Gamma[\mathbf{g}\times]^T(\mathbf{H} - \mathbf{H}_d) \tag{9}$$

where $[\mathbf{g}\times]^T$ is the transpose of the cross-product matrix representation of the gravity vector. In order to eliminate the possibility of singularities in the solutions to the kinematic equations, the author chose a quaternion representation of the simulator orientation.

The spacecraft equation of motion can be written as

$$\dot{\mathbf{H}} + [\omega\times]\mathbf{H} = -m[\mathbf{g}\times](\mathbf{r}_0 + \delta\mathbf{r}_2) \tag{10}$$

where ω is the system's angular velocity. Using the same combined feedback and feedforward momentum tracking control law proposed in [34],

$$\tau = -K(\mathbf{H} - \mathbf{H}_d) + [\omega\times]\mathbf{H} + \dot{\mathbf{H}}_d \tag{11}$$

where τ represents a torque, and K represents a gain matrix, it is possible to set Equation (11) equal to the right-hand-side of Equation (10) in the following manner.

$$-m[\mathbf{g}\times](\mathbf{r}_0 + \delta\mathbf{r}_2) = -K(\mathbf{H} - \mathbf{H}_d) + [\omega\times]\mathbf{H} + \dot{\mathbf{H}}_d \tag{12}$$

Allowing $\mathbf{r}_0$ to be equal to $\begin{bmatrix} 0 & 0 & 0 \end{bmatrix}^T$, and solving for $\delta\mathbf{r}_2$ it is determined that

$$\delta\mathbf{r}_2 = \frac{-1}{m}[\mathbf{g}\times]^+\left(-K(\mathbf{H} - \mathbf{H}_d) + [\omega\times]\mathbf{H} + \dot{\mathbf{H}}_d\right) \tag{13}$$

where $[\mathbf{g}\times]^+$ denotes the pseudoinverse of the cross product representation of the gravity vector. The pseudoinverse of a generic matrix A satisfies

$$\begin{aligned} AA^+A &= A \\ A^+AA^+ &= A^+ \\ (AA^+)^* &= AA^+ \\ (A^+A)^* &= A^+A \end{aligned} \tag{14}$$

where A^* represents the conjugate transpose of the matrix A [40]. The pseudoinverse generated in SIMULINK is calculated via singular value decomposition.

Note the similarity between the above solution and the the generic equation $A\mathbf{x} = \mathbf{b}$. In this case

$$\begin{aligned} A &= -m[\mathbf{g}\times] \\ \mathbf{x} &= \delta\mathbf{r}_2 \\ \mathbf{b} &= -K(\mathbf{H} - \mathbf{H}_d) + [\omega\times]\mathbf{H} + \dot{\mathbf{H}}_d \end{aligned} \tag{15}$$

There is not a unique solution, since $\mathrm{Rank}([\mathbf{g}\times]) = 2$, i.e., rank deficient, and the $\dim(\delta\mathbf{r}_2) = 3$.

With just the balance masses, it is not possible to create torques about the gravity vector. For example, if the simulator were oriented with pitch, roll and yaw values all being zero, this method would not be able to generate a torque around the yaw, or vertical, axis.

The integrated value for $\delta\mathbf{r}_1$ from Equation (9) was summed with $\delta\mathbf{r}_2$ from Equation (13) to find

$$\delta\mathbf{r} = \delta\mathbf{r}_1 + \delta\mathbf{r}_2 \tag{16}$$

This final CG compensation vector, $\delta\mathbf{r}$, accounts for the Lyapunov function trajectory which the simulator must follow and the manner in which the control law must be implemented, that is by angular momentum inputs made by deviation in balance mass positions only.

3. Simulation

An initial simulation was run in order to establish the limits of controllability of the balancing system. Masses were assigned to four objects: the three balance masses and the entire system without the balance masses. Values were calculated for $\mathbf{R}_i$, $\mathbf{r}$, and $\Delta\mathbf{d}$ from Equations (1-3). Iterations of initial CG offset showed that the offset, along each axis, needed to be less than a value on the order of 0.3 mm in order for the automatic system to be capable of collocating the CG with the COR.

In order to validate the automatic mass balancing technique suggested here, a computer simulation was developed. All sensor inputs were simulated in SIMULINK. Initial estimates for mass and inertia values for this thesis were computed using an NX6 CAD model. Iterative corrections for COM compensation were made within the SIMULINK modeling environment.

The commanded perturbation signals chosen used to generate the desired angular trajectory were three identical inputs into each channel and can be written as

$$\phi = 15e^{-kt}\sin(\frac{1}{10}t)$$
$$\theta = 15e^{-kt}\sin(\frac{1}{10}t) \quad (17)$$
$$\psi = 15e^{-kt}\sin(\frac{1}{10}t)$$

where ϕ, θ, and ψ represent roll, pitch and yaw angles, respectively. Other values used in the simulation are included in Table 4.

Sample Time, t_s	0.01 sec
Duration, t_f	3000 sec
Time Start, t_0	5 sec
Total Mass, m	7.798 kg
Individual Balance Masses, m_1, m_2, m_3	0.2 kg
Initial CG Offset, $\mathbf{r}_0$	$\left[-0.235,\ 0.861,\ 0.467\right]^T \times 10^{-3}$ m
Simulator Moment of Inertia, J	$\begin{bmatrix} 70864.935 & 0 & 0 \\ 0 & 76892.989 & 0 \\ 0 & 0 & 39773.049 \end{bmatrix} \times 10^{-6}\ \mathrm{kg \cdot m^2}$
Maximum Balance Mass Deviation, d_i	10 mm
Maximum Rate of Balance Mass Movement	4 mm/s
Initial Angular Velocity, ω_0	$\begin{bmatrix} 0 & 0 & 0 \end{bmatrix}^T$
Gain Matrix for Excitation, K	$\begin{bmatrix} 10 & 0 & 0 \\ 0 & 10 & 0 \\ 0 & 0 & 10 \end{bmatrix}$
Initial Attitude	$\phi = 0,\ \theta = 0,\ \psi = 0$
Unit Vectors, u_i	$u_1 = \begin{bmatrix} 1 & 0 & 0 \end{bmatrix}$ $u_2 = \begin{bmatrix} 0 & 1 & 0 \end{bmatrix}$ $u_3 = \begin{bmatrix} 0 & 0 & 1 \end{bmatrix}$

Table 4. Values Used in Simulation

The system is initially left unperturbed for an initial period, on the order of 5 seconds, as the system may rest on the test-bed once released by an operator moving to the control terminal to initiate the mass-balancing program. The control inputs, the commanded balance mass positions, are calculated and sent to the “simulator” for a period on the order of 50 minutes. The following figures demonstrate the ability of the control system to bring the simulator under control, and leave it in a stable condition. In order to validate these results, a test-bed is being constructed in the NACL.

The $\mathbf{H} - \mathbf{H}_d$ term, introduced in Equation (8) is plotted over time in Figure 15. This plot shows short-lived transients with settling times on the order of 20 seconds. The CG offset vector, $\mathbf{r}$, from Equation (2) is shown plotted over the first 25 seconds in Figure 16. No inputs are made to the system over the first 5 seconds. Some transients with settling times similar to those shown in Figure 15 are also noted here. Angular momentum of the simulator, $\mathbf{H}$, from Equation (10), is shown in Figure 17. Note the steady maximums in this parameter after the first 20 seconds. The CG offset vector is shown in Figure 18 to settle quite well as the simulation progresses. Figure 19 shows that over the final 500 seconds of the simulation, the offset has consistent maximums of less than $3 \times 10^{-6}\ \mathrm{m}$. The magnitudes of the oscillations shown in Figure 19 relate directly to maximum values of CG offset once the automatic mass balancing system is deactivated. As discussed further in Chapter 3, the required residual torques must be less than values on the order of $2 \times 10^{-4}\ \mathrm{N \cdot m}$. As demonstrated in Figure 20, these results show, at least in simulation, that achieving this goal may be possible.

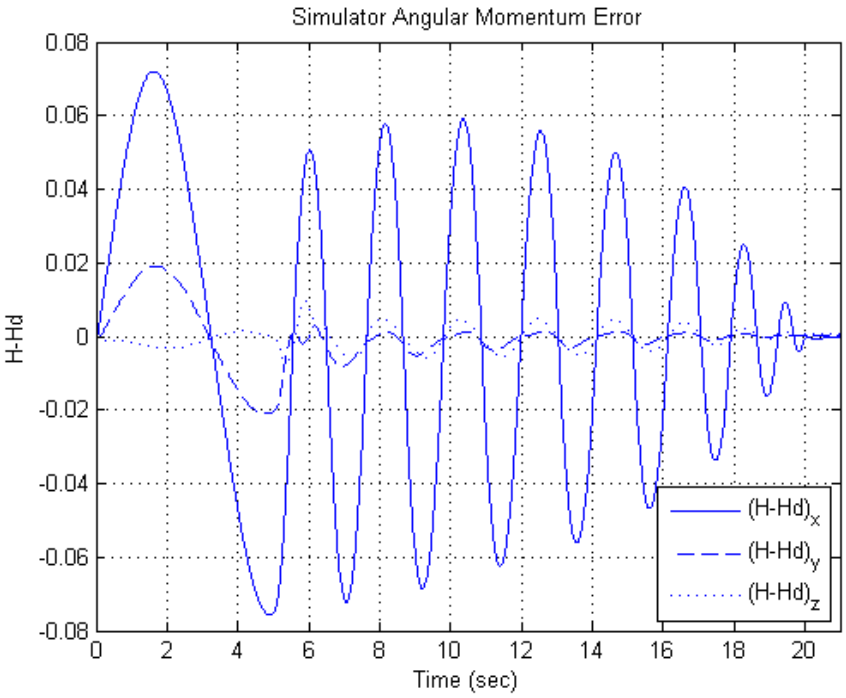

Figure 15. Angular Momentum Error Transients

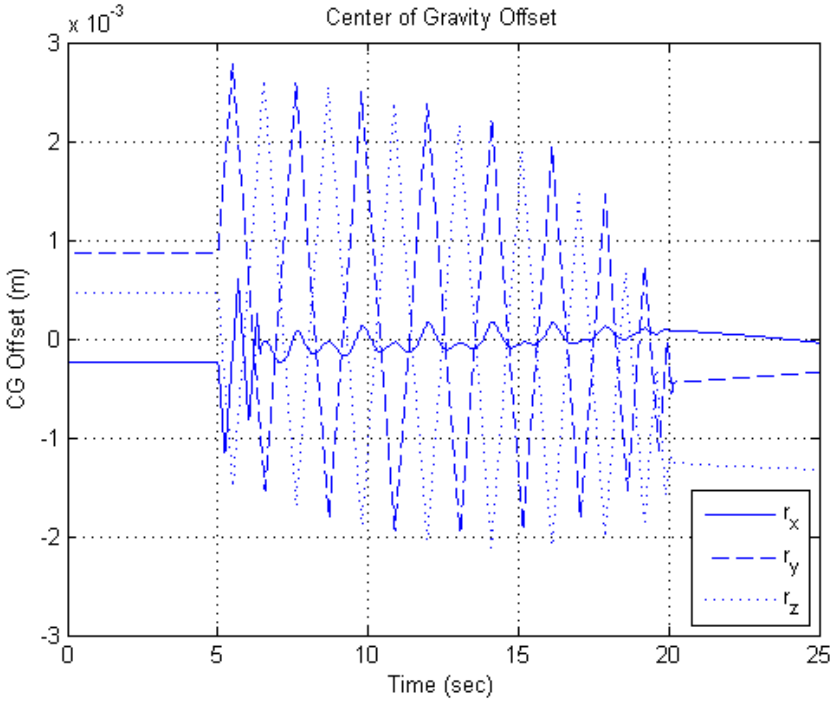

Figure 16. Center of Gravity Offset Transient

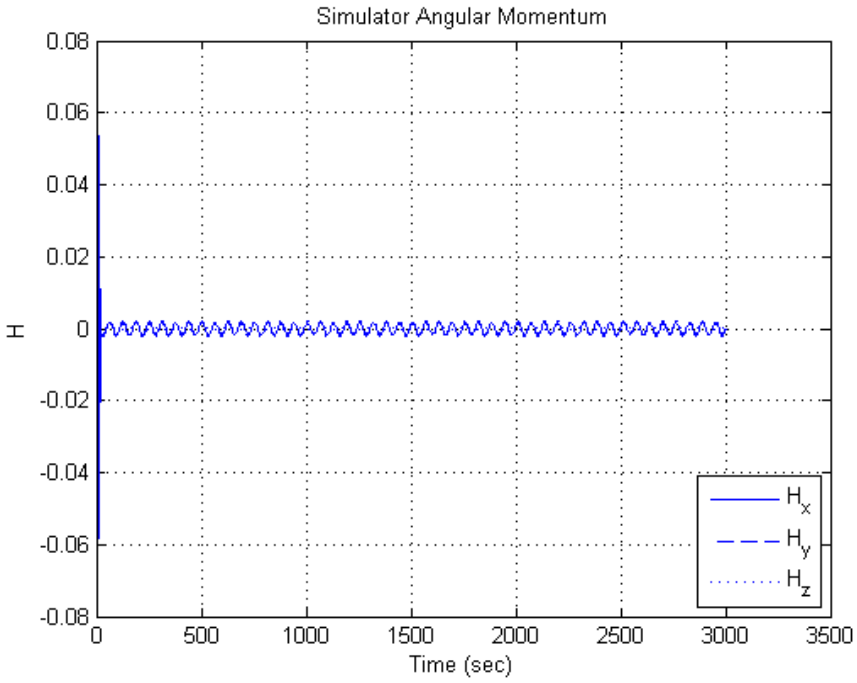

Figure 17. Angular Momentum

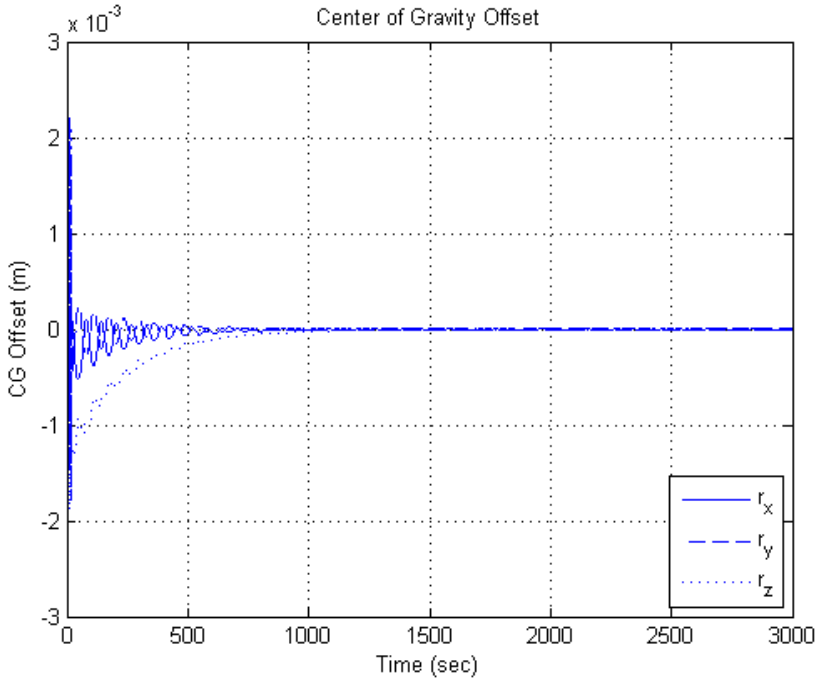

Figure 18. CG Offset

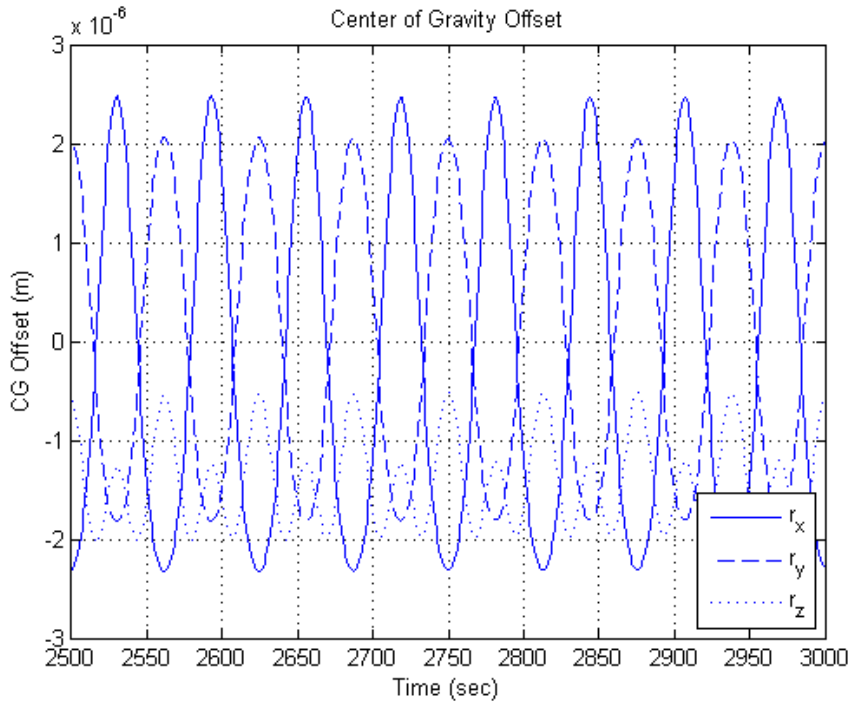

Figure 19. Center of Gravity Offset

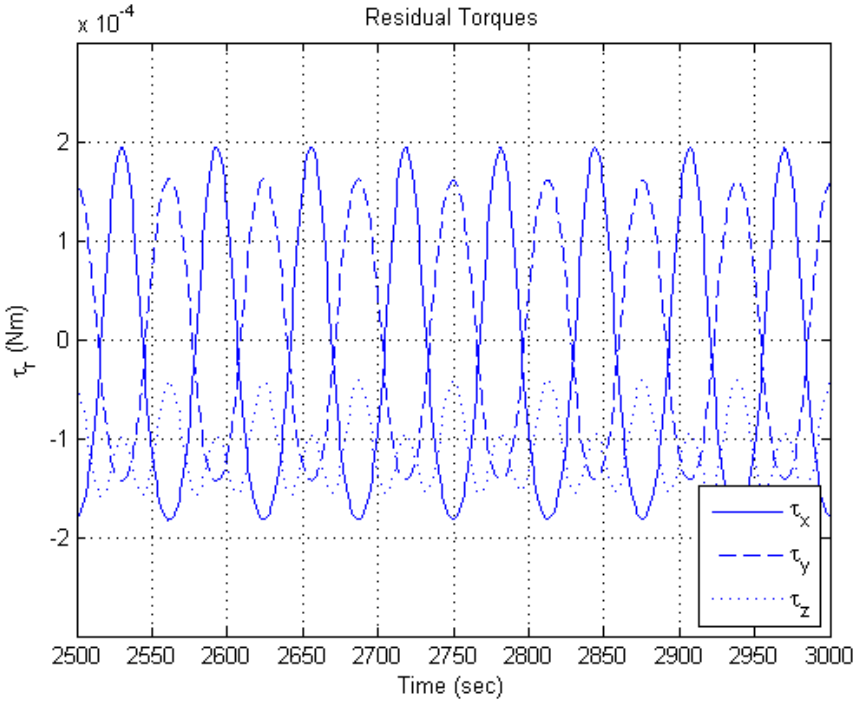

Figure 20. Residual Torques

THIS PAGE INTENTIONALLY LEFT BLANK

III. ADCS TEST-BED DESIGN

A. INTRODUCTION

The CubeTAS consists of a hemisphere over a spherical air-bearing with two parallel discs connected by four aluminum threaded rods. The lower disc was designed with a 10 cm cube in its center providing a modular space for future cubesat form factor components to be added. System components are firmly mounted to each of the discs and to the outside of the 10 cm cube.

In the design, it was important to provide significant rigidity to the structure in order to reduce the effects of the flexing with varying attitude configurations. In order to be able to control the COM along each of the primary coordinate axes, three masses, of significant mass, were selected and connected to linear motors. Electronics, capable of powering and controlling the mass position, were strategically mounted keeping the COM as close as possible to the COR of the acrylic hemisphere, in addition to various sensors required for closed loop control. Figure 21 shows a general layout of the simulator and Appendix B lays out the main components and parts required to construct the system.

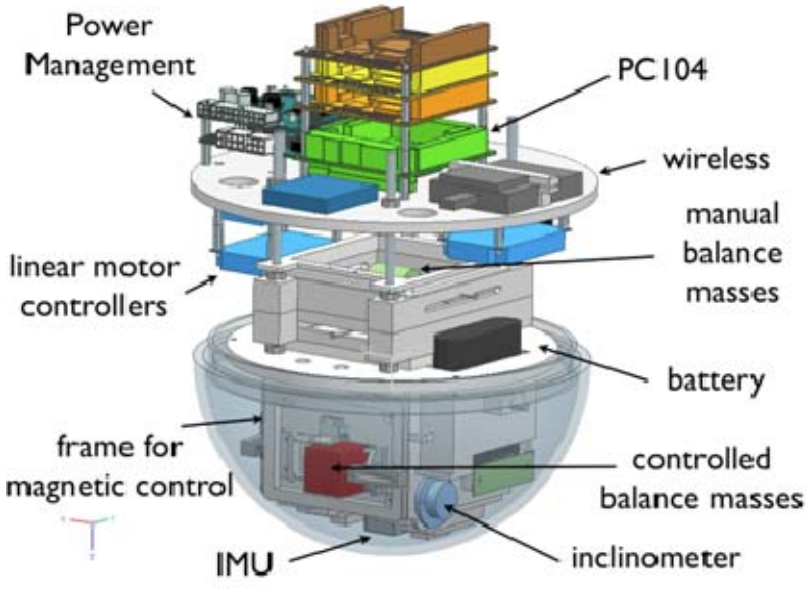

Figure 21. Cubesat Three-Axis Simulator (CubeTAS)

The test-bed maintains all required components in or above an acrylic hemisphere. Unique attachment hardware is mounted on a polycarbonate structure generated in a Stratasys Fortus Fused Deposition Modeling (FDM) 400mc prototyping machine [41]. This hemisphere is placed atop the spherical air-bearing supported by the aluminum structure shown in Figure 22. The air-bearing is in the center of the black ring at about knee height in Figure 22. Further discussion will provide a more in depth description of the test-bed.

Figure 22. Aluminum Support Structure

For attitude determination, data from a combination of two single-axis inclinometers, one three-axis Inertial Measurement Unit (IMU), and one sun sensor will be integrated in 2010 through the implementation of an Extended Kalman Filter (EKF).

A PC/104 is used to run the required data acquisition algorithms and route all associated control signals to components either directly or through a digital to analog PCB. Position commands are sent to the linear motors based on feedback collocating the CG with the test-bed's COR.

Power is supplied by an on-board battery, which can be recharged as necessary, supplying the variety of voltages required by each of the components.

B. COMPONENTS

1. Structural

a. Spherical Air Bearing

A spherical air-bearing allows the test-bed to be supported by a thin film of pressurized air and lifted out of contact with supporting structures. This eliminates friction aside from that associated with air contacting the surface of the hemisphere and drag as the airflow separates from the test-bed. In addition to 'zero friction' behavior, the air bearing eliminates wear and lubrication problems of standard bearings.

The air bearing purchased (Figure 23) is compatible with a 5-inch outer diameter (OD) sphere. The operating fly height is 0.0127mm (0.0005") with a 68 kg (150 lbf) load at 80 psi [42]. The maximum supply pressure is 120 psi.

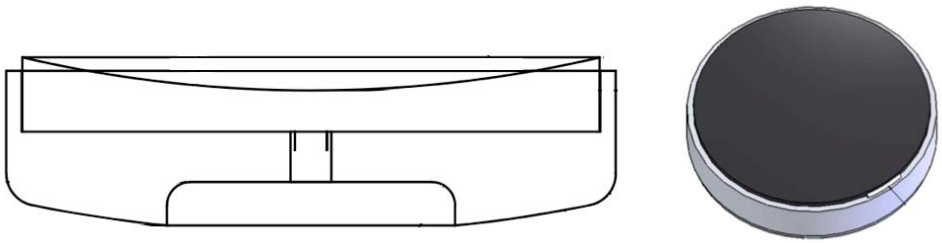

Figure 23. CubeTAS Spherical Air Bearing (After [42])

New Way Air Bearings' Porous Media Technology provides an evenly distributed airflow across the entire surface with "10s of millions of sub-micron pores evenly spaced across the surface of the bearing [43]." Figure 24 shows five different air bearings and their associated pressure distribution patterns.

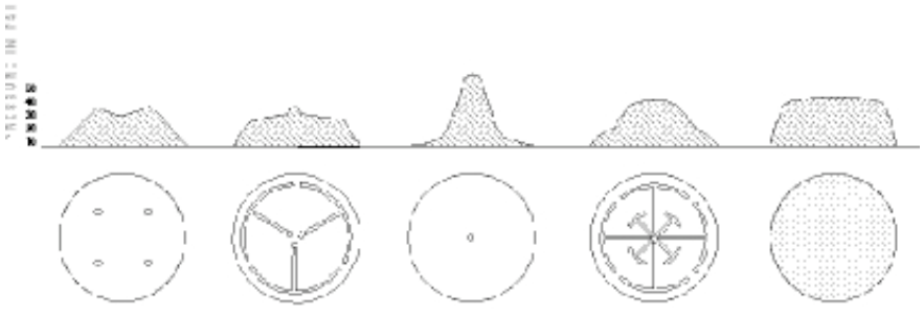

Figure 24. Pressure (psi) vs Lateral Position of various air bearings; From left to right: 1) Multiple orifices with no grooves, 2) Multiple orifices with distribution grooves, 3) Single orifice, no grooves, 4) Single non restrictive input port with depth and width of grooves providing restriction, 5) Full porous face with 10s of millions of sub-micron pores evenly spaced across the face (From [43])

b. Aluminum Support Structure

A structure was designed in order to support the test-bed above the floor allowing pressurized air to be routed to the bottom of the spherical air-bearing without varying the pre-existing magnetic field around the test-bed. An aluminum 80/20 material was chosen for its modularity and ease of construction. TECO Pneumatics, Inc., was sent a preliminary sketch (Figure 25) and returned a CAD draft interpretation of the author's intent (Figure 26).

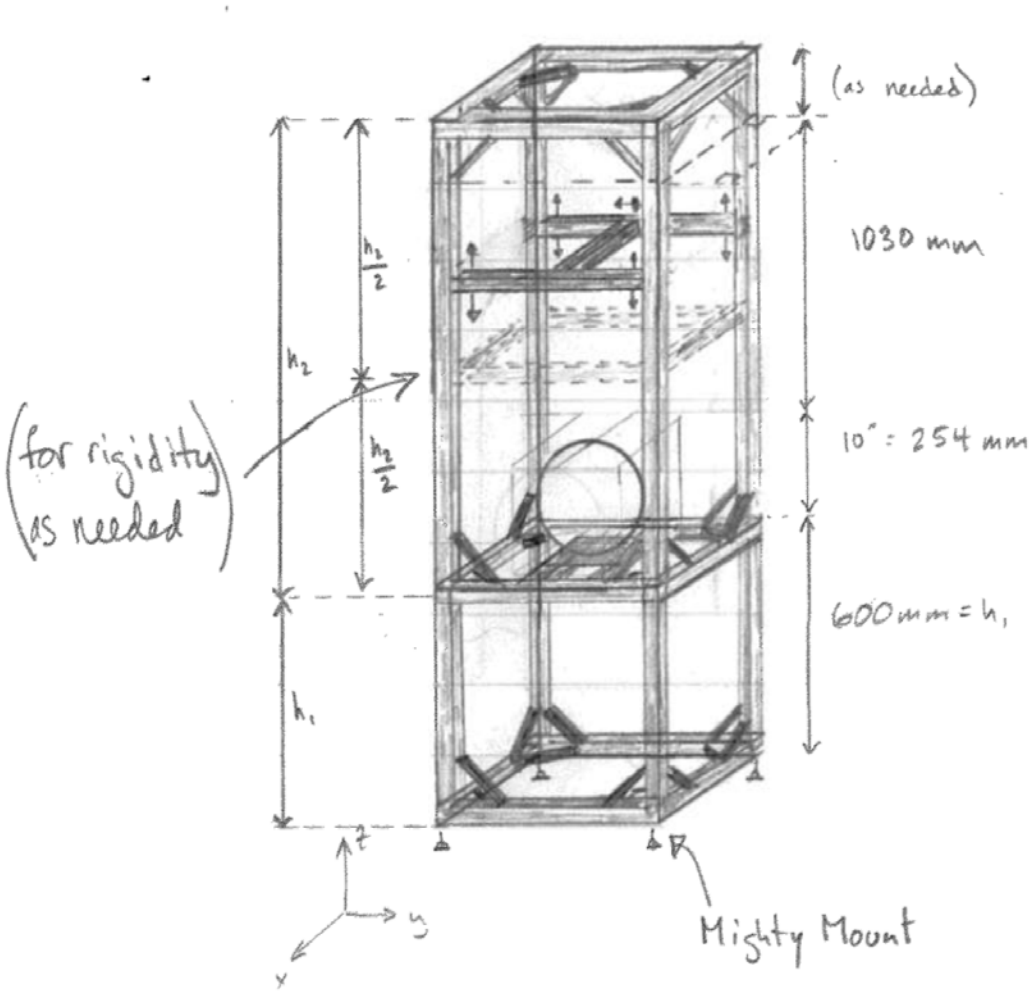

Figure 25. Aluminum Support Structure Preliminary Sketch

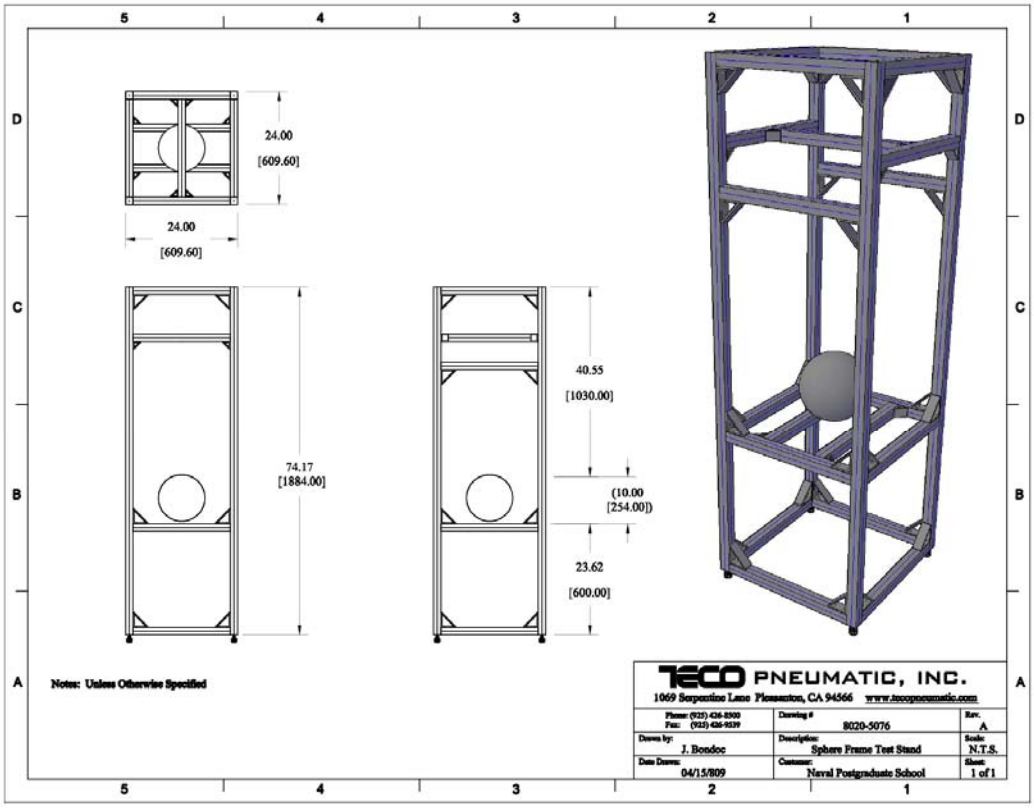

Figure 26. TECO Pneumatics, Inc., Draft of the Aluminum Support Structure (From [44])

This design was the 5th iteration of the structure. Other designs considered are shown below. The first iteration attempted to use minimal material in the design with a ring around a sphere keeping it on the air bearing. A sphere was modeled through all design iterations until it was learned that limitations prohibited the use of a full sphere. Limitations included an unavoidable disturbance in air flow associated with the joining point of two hemispheres and increased complexity associated with having only minimal components inside the sphere. The advantage of using COTS parts is the ability to very quickly integrate them, as originally intended, in the test-bed. If we attempted to include our linear motors, for example, inside the sphere and its associated COTS controller outside the sphere, we would need an A/D board to measure signals from the proprietary equipment and send them wirelessly to a

external desktop for processing. This complexity was removed by accepting the addition of all parts associated with a component to the test-bed and the removal of the top hemisphere.

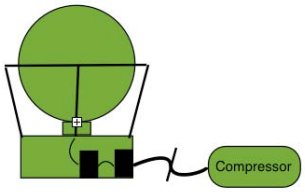

Figure 27. Structure: Version 1

The second iteration included the integration of a two-camera 3D motion analysis system and a safety net. The net was intended to eliminate visual obstructions in the cameras' field of view (FOV).

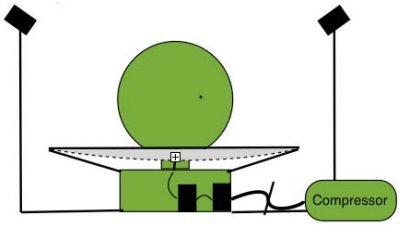

Figure 28. Structure: Version 2

The 3rd iteration was intended to raise the structure, allowing it to be independently supported, without the requirement of an external table. This also allowed the structure to be manually leveled with vibration dampening padded feet. The 3rd design was considered with the sphere at a standard table height or slightly higher allowing room for a net to catch the sphere in the case of instability causing it to fall from the air bearing. The raising of the air bearing would have helped protect the sphere from scratches associated with contact of the structure during a fall.

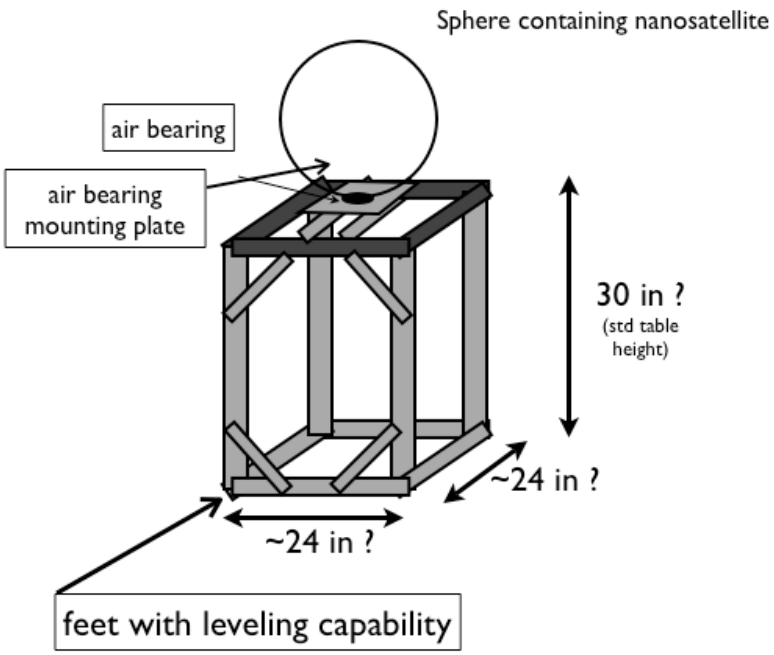

Figure 29. Structure: Version 3a

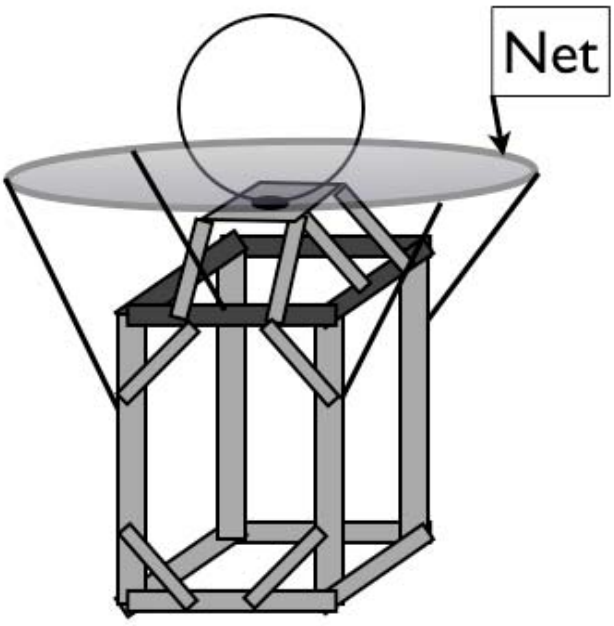

Figure 30. Structure: Version 3b

The 4th iteration eliminated the net and again placed the camera system above the sphere on a length of 80/20 that can be adjusted in the vertical and one lateral dimension. This design was eliminated on account of the likelihood of vibrations affecting camera performance. Instead, a “cage” type design was considered and ultimately chosen for production (Figure 26).

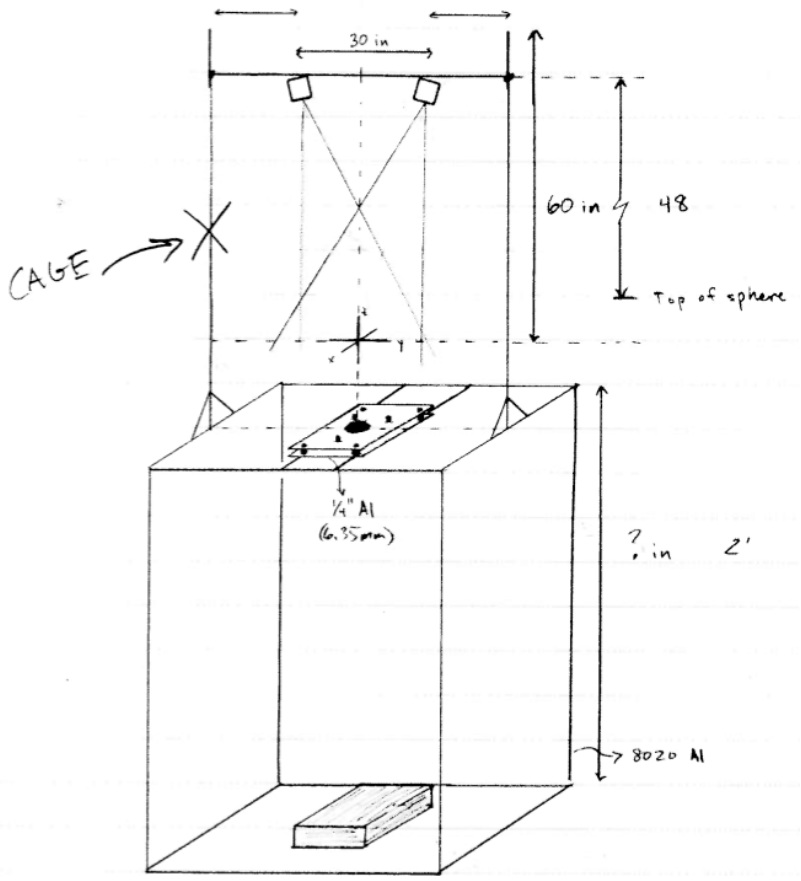

Figure 31. Structure: Version 4; Dimensions in inches

The cross sectional type chosen was the 40-4040 Lite (Figure 32) which has moment of inertias, in x and y, of 9.39 cm^4 [45]. The structure is made of 6105-T5 aluminum with cavities in each of the four corners giving it a reduced weight per meter of 1.78 kg/m. The aluminum, a paramagnetic material, provides the strength and rigidity desired without the negative sensitivity to external magnetic fields as ferromagnetic metals. Aluminum has the added benefit of decreased purchase cost and shipping expense.

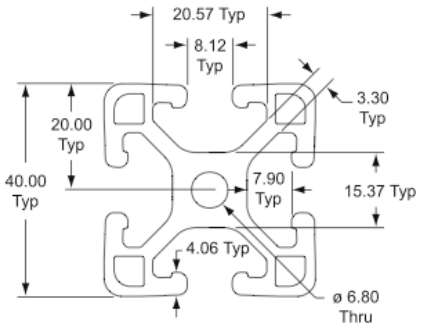

Figure 32. 80/20® Inc. 40-4040 Lite (From [45]); Dimensions in mm

c. Air Bearing Mount

The method chosen to mount the spherical air bearing is two ¼" aluminum plates, each with a hole removed from the center. The top plate has a larger hole in the center providing just enough room for the air bearing to be exposed while providing a restriction to motion in the vertical dimension with a shallow 1.24 mm lip (Figure 33). The bottom plate provides access for the pressurized air port. Both of the plates are attached at each corner and mounted to the structure via a roll-in T-nut.

Figure 33. Air-Bearing Mounting Plates; top view (left), side view (center), and bottom view (right)

d. Bumper

A protective bumper was added to prevent the simulator from falling from the structure as the result of a small-unexpected lateral impact. The bumper is designed to increase the distance the CG would need to travel before

reaching a point in which the simulator would fall from the platform supporting the air bearing. A net was initially conceived, but standard insulating foam for pipes was used as a simpler, cheaper option. The bumper is supported by four screws attached to the spherical air-bearing mounting plates (Figure 34).

Figure 34. Test-bed Protective Bumper

e. Hemisphere

As mentioned above, a sphere containing test-bed components was intended initially in order to provide 360° of freedom around each coordinate axis. A 2040-10V glass sphere was purchased from Teledyne Benthos Flotation (Figure 35) with the intention of removing the rubber seal from the "equator" and smoothing the transition between the two hemispheres.

Figure 35. Teledyne Benthos 2040-10V Glass Sphere (From [45])

Unfortunately, when the sphere arrived it was not smooth and was manufactured with two elevated regions at each of the “poles”. After a thorough search, it was determined that smoothing the 0.0508mm (0.002”) raised surfaces to the required RMS16 surface roughness would be inaccurate by hand and cost prohibitive using optics tooling.

California Quality Plastics was able to manufacture an acrylic sphere of the proper specifications for an affordable price. The first sphere ordered could be split into two halves with a lip along each half’s rim allowing them to join together. The idea with this design was to utilize a separate disc or plate of some sort to mount our components on and rigidly attach this to the centerline or equator of the sphere. This concept was again cost prohibitive and California Quality Plastics was asked to design a sphere with a disc mounted in the center. This final design was accepted after one iteration, to the same company, for a version much smoother than the first. The author has been unable to obtain the exact specifications on the sphere other than personal physical measurements. In addition to this uncertainty, two spheres of the final specifications were ordered and the method of manufacturing prohibits the finished product from matching the requested design exactly. Consequently, physical measurements should suffice as adequate.

The sphere, delivered as two halves, was separated and only the bottom portion used. As a whole, the acrylic sphere is actually a prolate spheroid with the following dimensions:

Outer radius	127 mm (5 in)
Thickness	6.35 mm (1/4 in)
Major axis	127 mm (5 in)
Minor axis	125.4 mm (4.94 in)
Flattening, f	0.012
Eccentricity, e	0.1576

Table 5. Spring Specifications

where the flattening and eccentricity are defined as

$$f = \frac{a-b}{a}$$
$$e = \frac{\sqrt{a^2 - b^2}}{a} \tag{18}$$

The main concern with using a prolate spheroid on a spherical air bearing is a variation in performance of the bearing based on the orientation of the sphere during operation. Based on rudimentary tests the air bearings performance is not degraded below angles below approximately 60°. This estimate is larger than that of other components that degrade the angular capability of the test-bed. A way to measure the actual radius of the sphere at various angles was not determined. Given the 1.27 mm (0.05 in) difference in radius between 0° and 90° pitch/roll, a disturbance in CG location will enter the system as the COR varies with pitch and roll variation. The effect of this disturbance will be explored further in experimental validation tests.

f. Polycarbonate Support

The author generated a few polycarbonate parts in NPS' 3D printer by first drafting scale models in CAD software. The models were transferred to the 3D printer, which uses two different tips to lay either polycarbonate or a

support material as appropriate to generate the parts. The polycarbonate is heated to around 300°C and laid layers with a thickness per layer of 0.254 mm [46].

The primary advantage of this technique is speed. Parts can be designed and generated within days, as opposed to weeks if you consider the time associated with shipping and machining similar aluminum parts. Some of the parts fabricated would have been impossible to create by any other method.

The primary disadvantage of this technique is quality control. Some of the smallest parts and attachment points on the test-bed require very accurate dimensions that were not within the capability of the 3D printer. Increased man-hours were expected, but a larger than expected amount of time was spent filing, drilling, and otherwise modifying printed components after production. Unfortunately, at least one component fractured as a result of the "clean up" process and had to be repaired with quick drying adhesive. Attaching hardware (about 8 nuts) had to be ground down due to inaccurate modeling of recess dimensions. The polycarbonate proved to be of too great a hardness (ASTM D785: R115) to be removed at the angles associated with getting the required tools to the recessed areas [46]. The working surfaces were within the 1U space reserved for future MEDs.

2. Electrical

a. Power

The battery chosen to power the CubeTAS on the test-bed was the Inspired Energy N2054HD26, 14.4V, 2.6Ah, 4 cell, Smart Standard Li Ion Battery Pack. Power is routed from the battery to a battery manager and DC/DC converter from which a number of voltages can be drawn.

The battery controller and regulated DC kit used is the EK-05 from Ocean Server. This system was integrated with the Inspired Energy N2054HD26 instead of the Ocean Server BA95HC-FL in order to save weight and space allowing the battery to be mounted with the majority of its weight below the x-y

plane of the simulator. Both batteries provide a 14.4 V DC source. Initial testing of this integration was conducted by Major Melone at NPS, while conducting his thesis work. His thesis was scheduled to be published at NPS in December 2009.

b. PC/104

The PC/104 board chosen was the Advanced Digital Logic ADLLX8PC–AMD Geode™ LX800. This board has a 500 MHz processor and a can run on a processor load of 0.9W. For cooling, a fanless heat sink was used to dissipate excess heat from the PCB. The Linux based OS runs on an integrated 4GB SSD flash [47]. Table 6 shows the other features of the ADLLX8PC.

500MHz Processor
Power Management (ACPI 2.0 & APM 1.2)
SoDIMM200 up to 1GB DDR-400
Built In 2GB SSD Flash (optional)
Built In Geode LX800 @ 0.9W
CRT/LCD on-board
10/100 Base-T LAN-Ethernet
4x USB V2.0 Ports
EIDE Hard Disk Interface
COM1, COM2, LPT1
RTC and Watchdog Timer
AC97 Sound Interface (in & out)
PC/104-Plus BUS Connector
Single 5VDC Power Supply

Table 6. Features of the Advanced Digital Logic ADLLX8PC–AMD Geode™ LX800 (After [47])

The PC/104 is responsible for receiving data from the sensors, via the analog to digital board in the case of the inclinometers, and using that data to compute desired balance mass locations and then sending commands to the squiggle motors via New Scale Technologies' own motor controller.

c. Serial Board

With an increased requirement for RS-232 connections, an Acces I/O Products, Inc., 104-COM-8SM Serial Communication Board was used to bridge the gap between our need for serial ports and the two COM ports provided by the PC/104. This serial board provides eight serial ports.

d. A/D Board

As the inclinometers are analog devices and our controls implemented digitally on the PC/104, we used an Analog to Digital board to convert the signals being sent to the ADLLX8PC.

The board chosen was the Diamond-MM-32-AT 16-Bit Analog I/O PC-104 Module with Autocalibration. Some of the features of the board are listed in Table 7.

Analog Input Channels	32
Analog Output Channels	4
Max Output Current	5mA
Max Sampling Rate	200 kHz
Digital I/O	24 bidirectional lines

Table 7. Diamond-MM-32-AT (After [48])

e. Relay Board for Magnetic Control

Passive magnetic control is envisioned as a possible control method on the test-bed with an external Helmholtz coil. In order to send the proper signals to the three coils on board, a relay board was mounted on the simulator. Coils have been installed on CubeTAS as shown in Figure 36. Another NPS student, working on magnetic control schemes, prepared the coils with approximately 400 windings each.

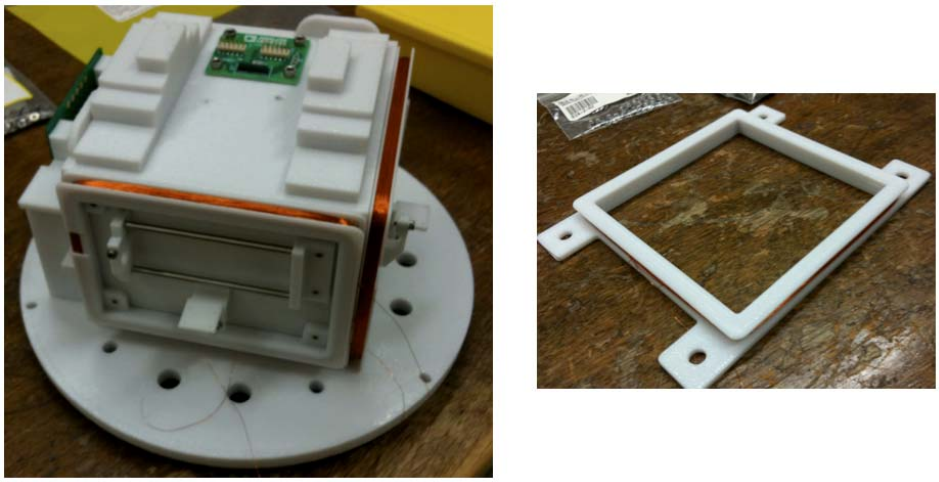

Figure 36. CubeTAS Magnetic Coils

3. Sensors

a. Inertial Measurement Unit

In order to collect acceleration, gyroscopic, and magnetometer data in all three axes, the ADIS16405/PCBZ, Figure 37, three-axis inertial sensor was purchased from Analog Devices, Inc. This Inertial Measurement Unit (IMU) uses a Serial Peripheral Interface (SPI) connection to the PC/104 and requires 5V of power supply. The capabilities of the IMU are shown in Table 8.

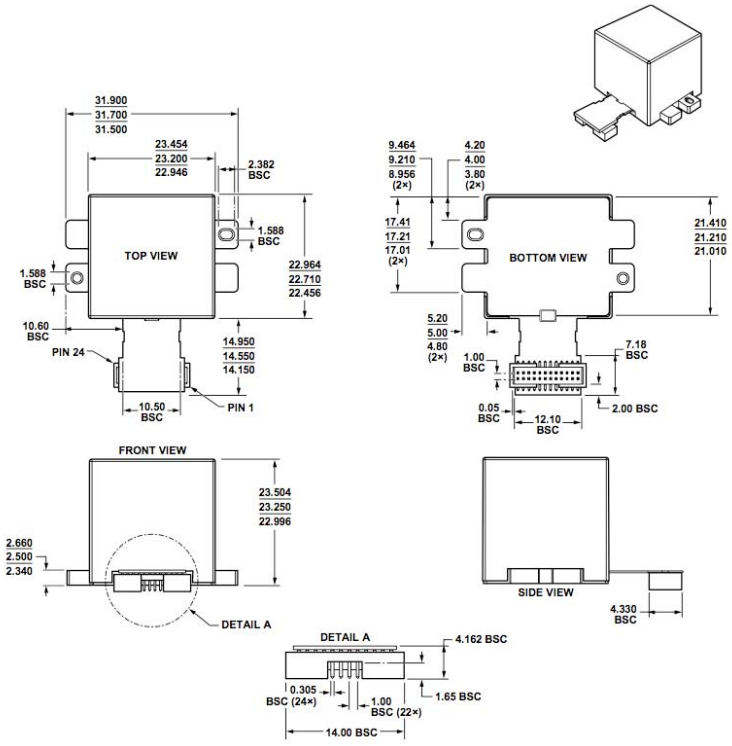

Figure 37. Analog Devices, Inc., ADIS16405/PCBZ (After [49])

Accelerometer	$\pm 18g$
Gyroscope (selectable)	$\pm 75°/\text{sec},\ \pm 150°/\text{sec},\ \pm 300°/\text{sec}$
Magnetometer	± 2.5 gauss
Operating Temperature Range	$-40°C$ to $+105°C$
Digitally Controlled Sample Rate	up to 819.2 sps (or up to 1200 with external clock)

Table 8. Analog Devices, Inc., ADIS16405/PCBZ Data (After [49])

The IMU is used on the NPS TINYSCOPE project for attitude determination.

b. Inclinometers

In order to gather real time angular position data from the simulator, two Rieker N4 inclinometers, Figure 38, were placed to gather data about the x and y axes of the system. With a transverse sensitivity of less than 1% at 30° tilt, there is minimal error expected form these sensors. Table 9 shows the capabilities of the N4 inclinometers. One of the advantages of these inclinometers is the aluminum mounting ring and the plastic housing, which reduce ferromagnetic effects on the test-bed.

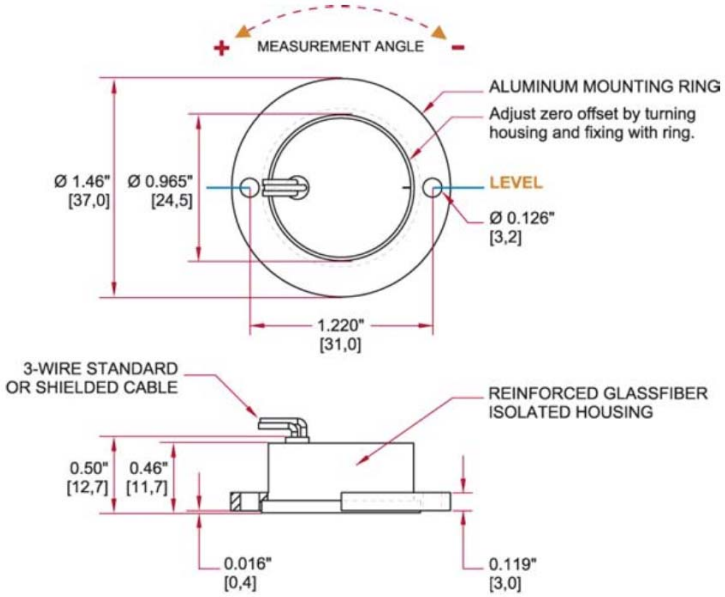

Figure 38. Rieker, Inc., N4 Inclinometer (From [50])

Measuring Range	$\pm 70°$
Resolution	$0.01°$
Max. Non-linearity	$< 0.2\%$ Full Range
Response Time	< 0.3 sec
Power Supply	$5V$ regulated
Current Consumption	Approx. $1\text{m}A$ at $5V$
Sensitivity	Approx. $3.2\text{m}V / °$
Temperature Drift of Sensitivity	$< \pm 0.025\text{m}V / C$

Table 9. Rieker, Inc., N4 Inclinometer Data (After [50])

c. Sun Sensor

In order to increase the accuracy of simulator angular orientation about the yaw axis, a SS-411 Two-Axis Digital sun sensor, Figure 39, from Sinclair Interplanetary is integrated into the test-bed with an external light source. The light source, not yet purchased, will provide parallel rays of incoming light for the sensor simulating rays of light, as they would arrive at the sensor from the sun on orbit. The sensor is mounted on the simulator at $90°$ from the horizontal with two light sources external to the simulator allowing accurate data collection from $0°$ to $360°$ in yaw. Other pertinent data is included in Table 10.

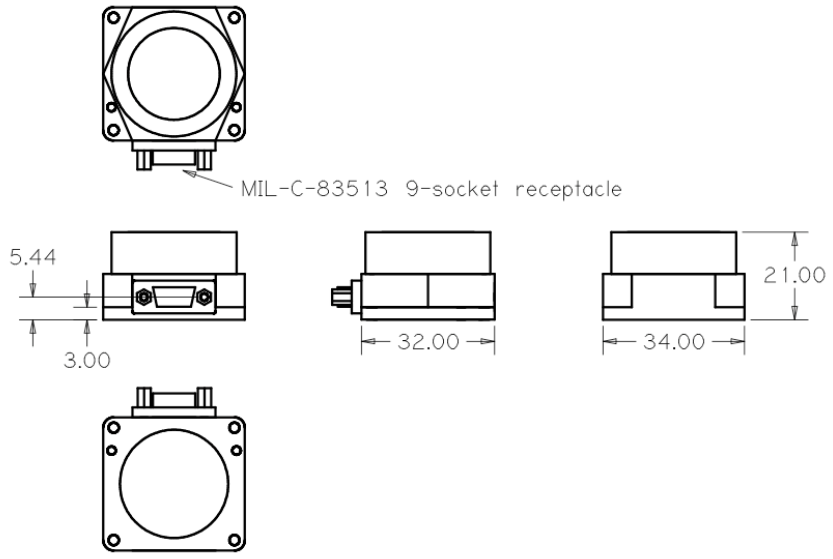

Figure 39. SS-411 Two-Axis Digital Sun Sensor Mechanical Drawing (mm) (From [51])

Accuracy	$\pm 0.1°$ over $\pm 70°$ Field-of-View
Bandwidth	5 vector solutions per second
Mass	34g
Supply Voltage	4 to 50 V
Supply Current	5.0 mA avg, 15.0 mA peak
Operating Temperature	$-25°C$ to $+70°C$

Table 10. SS-411 Two-Axis Digital Sun Sensor Data (After [51])

d. Camera System

There are future plans to integrate an external camera system capable of accurately determining simulator attitude in three dimensions. Spica Technologies, Inc., is capable of providing a system with two cameras with 8 or 12.5 mm lenses depending on calibration requirements. These cameras would be placed approximately 2–4 feet above the simulator in a configuration similar to that shown in Figure 40. Markers would be placed on the simulator in order for each camera to locate each in three dimensions. Although this system would

provide a spatial accuracy of the markers on the order of 0.03%, for the present this system is cost prohibitive [52]. Another version of the same system is being considered at almost half the cost.

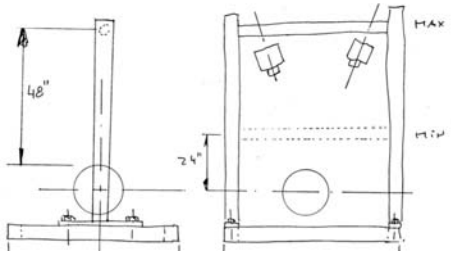

Figure 40. Potential Camera System for Angular Determination (After [53])

4. Actuators: Linear Motors

In order to precisely move the three balance masses of the system, each along its own direction vector parallel to each coordinate axis, three SQL-3.4-10 linear motors, Figure 41, were purchased from New Scale Technologies, Inc. These motors are capable of a resolution of .5 μm and operate with an integrated position encoder also provided by New Scale Technologies [54]. Additional data related to the SQL-3.4-10 is shown in Table 11. Linear encoders were also purchased from New Scale Technologies.

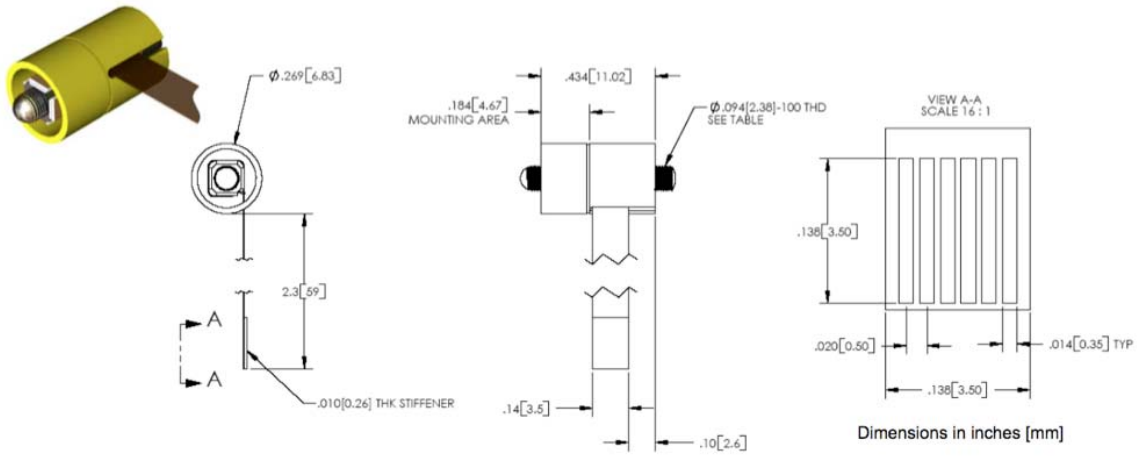

Figure 41. New Scale Technologies, SQL-3.4-10 (From [54])

Range	20 mm
Stall Force	200 g (2N)
Speed	4mm/s
Resolution	0.5 μm
Input Power to controller (moving)	1.6 W (varies with load and speed)
Operating Temperature	$-30°C$ to $+80°C$
Weight	1.7 g

Table 11. SQL-3.4-10 Data (After [54])

During the design process, three motors were evaluated as potentials for the test-bed. The most capable and also the most expensive option here was the LEGS motor by the Micromo Company. The next best option was the SQL-3.4-10 Squiggle motor by New Scale Technologies. A third option was considered from the Frigelli Company, the PQ-12.

The LEGS motor met all the size and resolution requirements. However, with a high price tag and a complicated control scheme, this motor was deemed infeasible.

The PQ-12 was very economical and compact, but did not provide the necessary resolution to remove all residual torques from the system. The following derivation demonstrates the inappropriateness of the PQ-12.

According to [55], it is appropriate to design a spacecraft simulator with residual torque, τ_r, one order of magnitude greater than the maximum planned on orbit disturbance torque, $\tau_{d\_\max}$, and two orders of magnitude less than the maximum attitude control torques of the spacecraft, $\tau_{c\_\max}$. With this consideration, this derivation uses a $\tau_{d\_\max}$ due to drag at 500 km altitude of $4 \times 10^{-6}\ \mathrm{N \cdot m}$ and an estimate for passive magnetic control for $\tau_{c\_\max}$ of $7.8 \times 10^{-7}\ \mathrm{N \cdot m}$.

From the onset, it is impossible to meet the recommendations of [55]. The test-bed must be controllable, so the inequality pertaining to the control torques was considered first. If residual torques are to be two orders of magnitude less than the maximum control torques, the required resolution capability of the linear motors must be on the order of $1.98 \times 10^{-10}\ \mathrm{N \cdot m}$. The only motor that came close to this resolution is the LEGS motor, but it was too expensive. It then became apparent that the project required an affordable motor with the smallest resolution possible.

A preliminary estimate of the mass of the simulator is 8 kg. If the COM is considered offset from the COR by some distance, d, then the following derivation can help as an aid in determining adequate motor resolution.

$$F = mg = (8kg)(9.81) = 78.5N \tag{19}$$

$$d = \frac{r_{es}}{2} \tag{20}$$

where d represents the moment arm and r_{es} represents the resolution of the motor.

$$\tau_r = Fd = F\frac{r_{es}}{2} \tag{21}$$

Therefore it is determined that if $\tau_r < 7.8 \times 10^{-7}\ \mathrm{N \cdot m}$, then $r_{es} \le 1.98 \times 10^{-10} m$.

With these initial estimates, the residual moment arm after balance mass positioning must be on the order of $2 \times 10^{-10} m$. The PQ-12 has a resolution of $2.5 \times 10^{-4} m$ and thus does not meet the requirements of this test-bed [56]. At almost a third of the cost of the LEGS motors, the SQL-3.4-10, with a resolution of $0.5\,\mu m$, comes the closest to meeting these requirements and was consequently the motor of choice for the CubeTAS.

The main drawback of the Squiggle motors was the requirement of a minimum preload of 10 grams (0.0981 N). This did not seem too stringent of a requirement at the onset, but when we started considering how to apply this preload in all test-bed configurations and not overload the motors at their 200

gram (1.96 N) maximum force capability, we quickly found more restrictions to the angular capability of the test-bed than we had originally foreseen.

A spring was considered in order to apply the required pre-load. The following derivation was conducted in order to determine the spring specifications required for the maximum angular capability of the test-bed. Figure 42 shows a side view sketch of a single balance mass mounted on two aluminum rods, the pre-loading spring on one side and the Squiggle motor on the other.

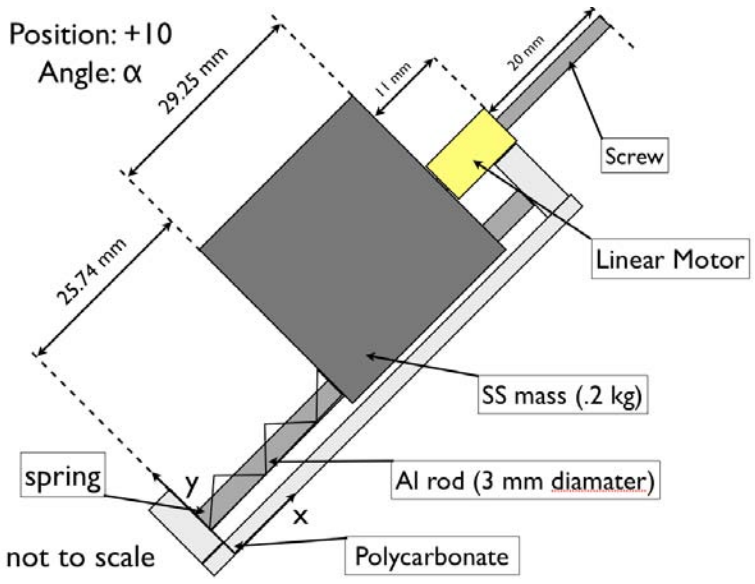

Figure 42. Balance mass at maximum lateral position and elevation

It can be shown that

$$\sum F_x = -(0.2)g\sin\alpha + F_{spring} - 0.01g \tag{22}$$

where the mass of the balance mass is 0.2 kg, g is the gravitational constant, and α is the angle between the local horizontal and the balance mass mounting plate. The third term represents the pre-load of 10 grams required by the motor to operate as designed. Solving for F_{spring} it can be determined that

$$\begin{aligned} F_{spring} &= (0.2)(9.81)\sin\alpha + (0.01)(9.81) \\ F_{spring} &= 1.962\sin\alpha + 0.0981 \end{aligned} \tag{23}$$

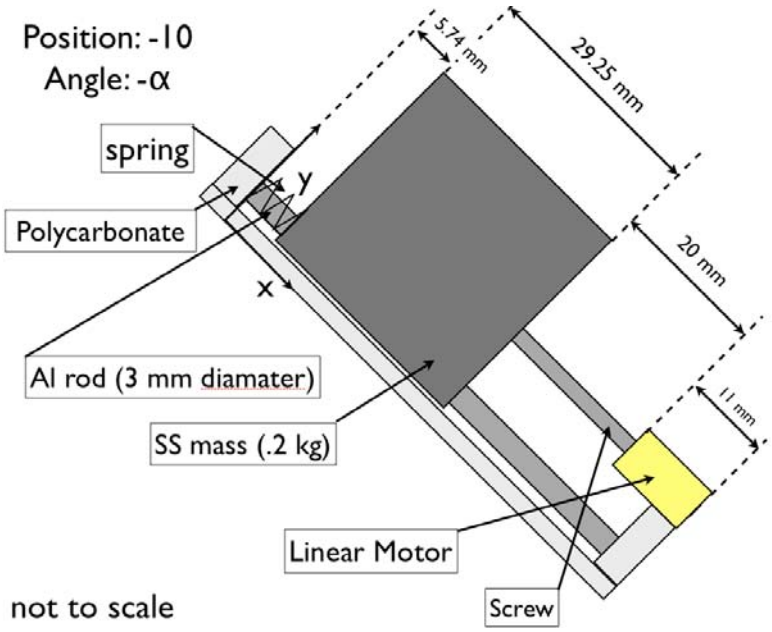

Figure 43. Balance mass at minimum lateral position and elevation

If the simulator rotates such that alpha becomes negative, Figure 43, it can be shown that

$$\sum F_x = \left(F_{spring} + 0.02k\right) + (0.2)g\sin\alpha - 0.2g \tag{24}$$

Substituting F_{spring} from equation (15) into equation (16) it is determined that

$$\mathrm{k} = \frac{\left(1.8639 - 3.924\sin\alpha\right)}{0.02} \quad \mathrm{N/m} \tag{25}$$

$$l_u = 0.02574 + \frac{\left(1.962\sin\alpha + 0.0981\right)}{k} \quad \mathrm{m} \tag{26}$$

where l_u represents the uncompressed length of the spring, and k represents the spring constant.

If an array of values for k and l are plotted for values of α, Figures 44–47, the maximum feasible angle of elevation, α, is approximately $25°$.

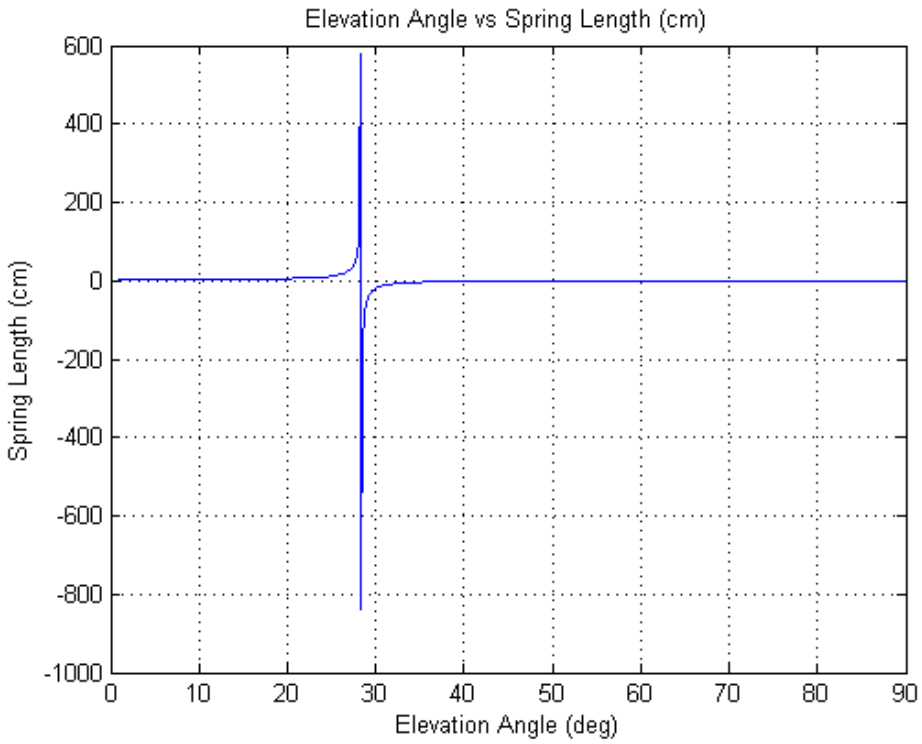

Figure 44. Angle vs. Length

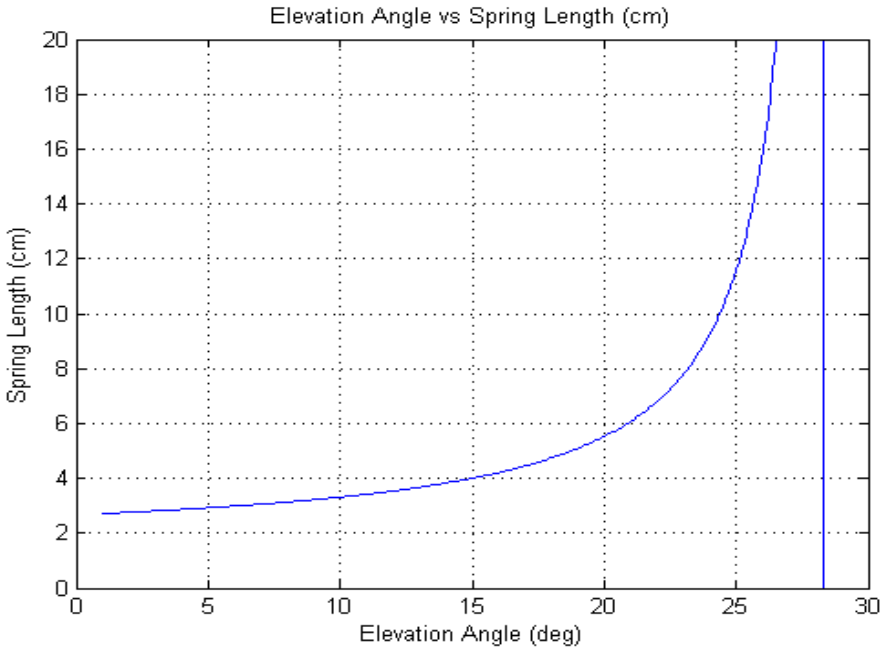

Figure 45. Angle vs. Length (0-30°)

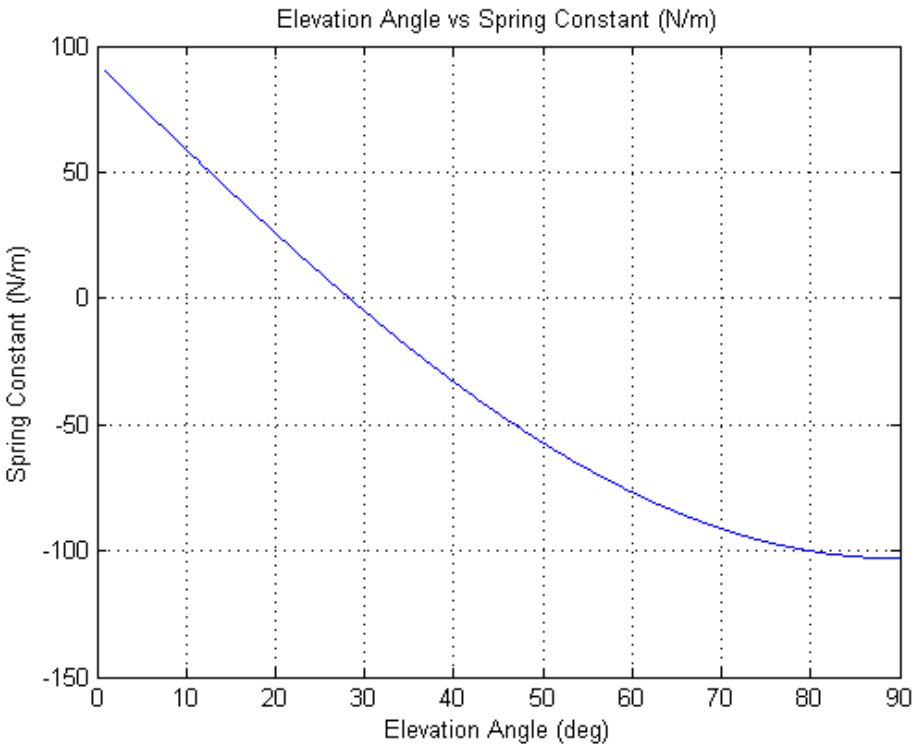

Figure 46. Angle vs. Spring Constant

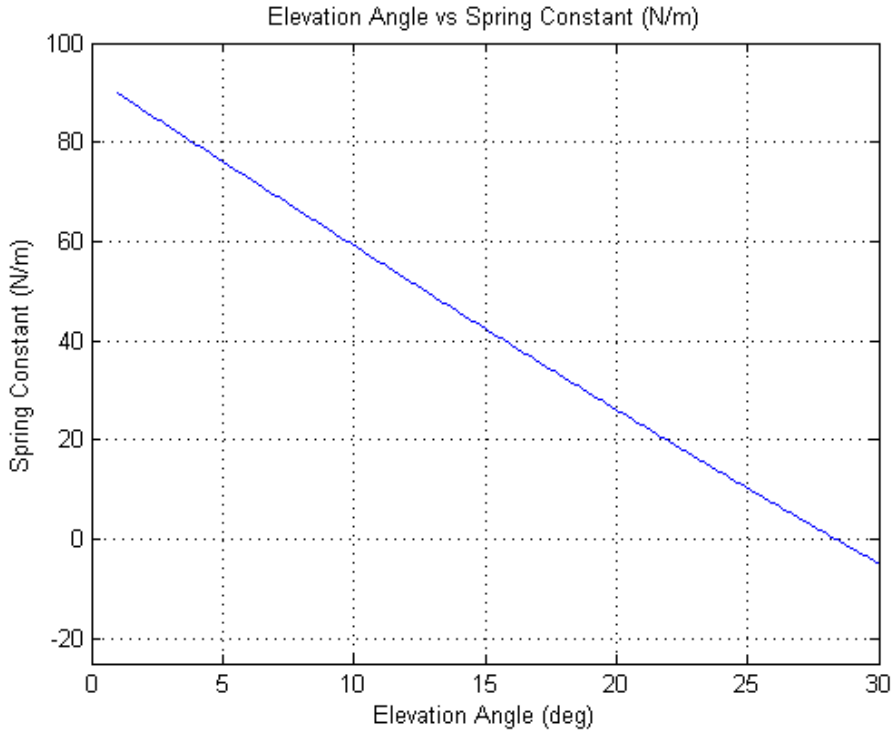

Figure 47. Angle vs. Spring Constant (0-30°)

The design specifications of the spring that would make the test-bed capable up to 25 degrees are:

Spring constant, k	0.01277 N/mm
Length uncompressed	11.5 cm
Length fully compressed	< 5.7 mm
Minimum Outer Diameter	3 mm
Maximum Outer Diameter	6 mm

Table 12. Spring Parameters for $\alpha = 25°$

After consultation with a few spring manufacturers, it became apparent that the spring required to meet the parameters in Table 12 would be too flimsy for most manufacturer's current tooling. Reducing the angular capabilities of the test-bed was to desired so another solution to the preload requirement was examined.

Instead of spring, a physical link between the balance masses and the squiggle motor was designed. This design uses gravity to apply the preload to the motor above approximately $2.5°$ in pitch and roll. Figure 48 shows the "arm" that is designed to be attached to one end of the balance mass and extends beyond the far end of the squiggle motor screw. This part was designed using English units to accommodate NPS machine shop requirements. The stainless steel balance masses are shown in Figure 49 with the attachment arms in the configuration required to apply the required preload.

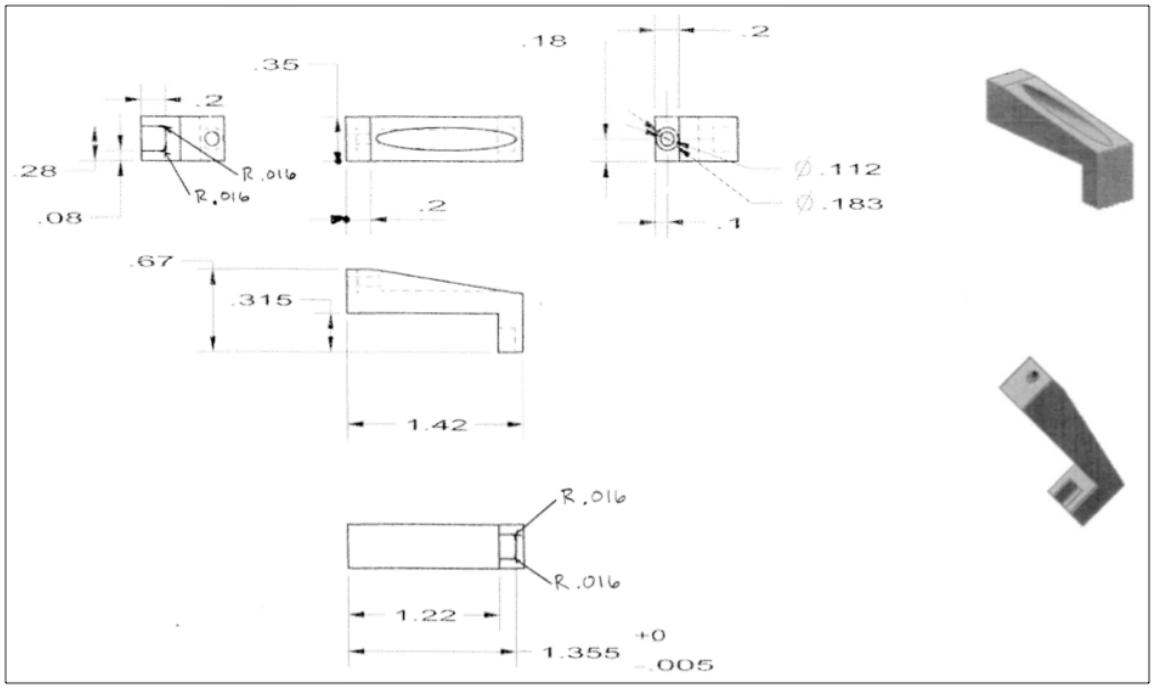

Figure 48. Arm that Attaches Balance Masses to Squiggle Motor (dimensions are inches)

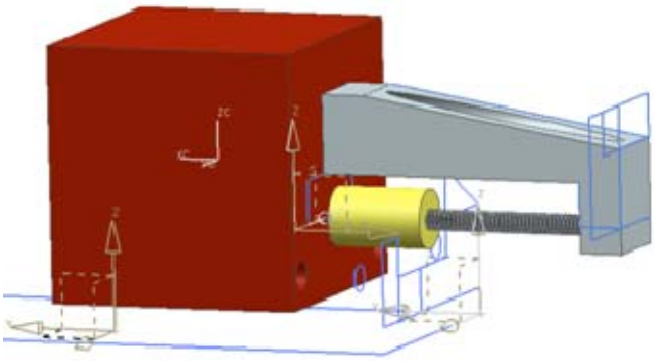

Figure 49. Stainless Steel Balance Masses with Attachment Arms

The main flaws in this design are friction between the motor shaft and the "arm" and motor position variability. Friction is reduced by the introduction of a Dupont™ Vespel® SP-21 in contact with either end of the Squiggle motor shaft. When the elevation angle shifts from positive to negative, there will be a shift in position of the balance mass when the contact point

between the motor and shaft shifts from one thread to the next. This will introduce an error on the order of 500 μm.

The error referred to above needs to be closely characterized and isolated so that it can be compensated for in the position control algorithm. One preliminary method of accomplishing this task may be to first position the balance masses appropriately to reduce gravitational torques to acceptable levels followed by deactivation of the automatic mass-balancing system. Second, it may be possible to command two of the Euler angles to constant values while commanding oscillations in the third and noting any deviation in encoder position from that which was commanded. Deviations in encoder position readings are expected at specific combinations of angle and mass position.

THIS PAGE INTENTIONALLY LEFT BLANK

IV. CONCLUSION

A. SUMMARY OF WORK COMPLETED

After a brief review of the Navy's use of satellites and a survey of three-axis simulators, an adaptive mass-balancing algorithm was developed. The design and approximately 90% of the construction of a three-axis simulator, for algorithm validation, was completed. This author's work will be followed another NPS student for further research and completion of the CubeTAS.

In order to develop the mass and inertia estimates in the CAD software NX6, the author made part models for over 100 parts. A few of the manufacturing companies shared their pre-made models, and although these parts could not be edited, they were very useful in specifying exact dimensions during the design process. Models were made for most of the nuts and screws in an attempt to make the model as legitimate as possible.

Parts were received and the test-bed constructed with reference to the CAD model. A 3D printing machine was used to manufacture many unique parts. One Squiggle motor was tested on a simple block of wood before being mounted to the final simulator. This test provided the author a place to examine the motor more closely and gain some hands on experience with the operation prior to integration on the CubeTAS.

The method of applying the preload to the Squiggle motor sets a minimum angular limitation to CubeTAS of approximately 2.5°. The maximum angular limit of the test-bed is still to be determined.

B. CONTRIBUTIONS

The main contribution of this thesis is the introduction of the first ever, to the best of the author's knowledge, Cubesat three-axis simulator that uses only the balance masses to balance the system. It may be possible for a CubeTAS to

be constructed at other universities to facilitate learning in other Aerospace departments giving students opportunities to test their own ADCS.

C. LESSONS LEARNED

Polycarbonate parts were first modeled in the NX6 environment and then exported for printing in the Stratasys 3D printer. All of the parts generated needed to be worked by hand, via manual drilling, or precision cutting instruments only available in the campus machine shop.

The logistics of ordering parts is a lengthy process. If corrections were to be made quickly, parts needed to be salvaged from old projects. If more accurate changes needed to be made, the timeline for construction of the CubeTAS moved the right with every delay.

In the design process, components were organized by weight and size. Wiring connections were considered during the design process but not enough allowance was made for the unknown.

V. RECOMMENDATIONS FOR EXPERIMENTAL VALIDATION

A. GENERAL METHODOLOGY

In order to effectively validate the simulation from Chapter II, it is essential to recreate the same conditions of the simulation. The SIMULINK model will be coupled with the sensors and actuators via S-functions that can be uploaded to the PC/104. Once each component is functioning properly, the system as a whole can be tested by running the simulation in real time on the simulator. The experimental results are compared to the results of the simulation so that the appropriate corrections can be made.

B. SYSTEM IDENTIFICATION

It is customary to conduct an experimental mass property identification of a spacecraft simulator. This process can provide more accurate inertia and center of mass estimates than those found using only computer modeling [55]. This data can be included in the real time mass-balancing algorithm. This thesis concludes with the use of CAD software to estimate inertia and center of mass values for CubeTAS. These CAD estimates were input into the simulation run in Chapter II.

C. RECOMMENDATIONS FOR FURTHER WORK

The first task that needs to be done in the continuation of this research is the generation of the S-functions required for each component to successfully communicate with the PC/104. The PC/104 can then implement the mass-balancing algorithm in real time on a Linux OS.

Another possibility for follow on work may be identifying the mass properties of the simulator once each of the sensors is effectively sending data to the PC/104 and commands can be sent to each of the actuators with reliable performance. This identification may include, but should not be limited to finding the simulators inertia matrix, J, and the CG location vector, $\mathbf{r}$.

THIS PAGE INTENTIONALLY LEFT BLANK

APPENDIX A: CUBESAT PARTICIPANTS LIST

Alabama	Auburn University	Luther Richardson	lrich@physics.auburn.edu
	University of Alabama		
	Tuskegee University	Vascar Harris	
Arizona	Arizona State University	Helen Reed	Helen.Reed@asu.edu
	University of Arizona	Mike Drake	drake@lpl.arizona.edu
Boston	Boston University	Don Wroblewski	dew11@bu.edu
California	Cal Poly State University	Jordi Puig-Suari	jpuigsua@calpoly.edu
	San Jose Sate University	Dick Desautel	dick.desautel@sjsu.edu
	Stanford University	Bob Twiggs	bob.twiggs@stanford.edu
	University of California Irvine	Divya Patel	
	University of California Santa Barbara	Marko Peljhan	
Colorado	University of Colorado - Boulder	Chris Koehler	Koehler@colorado.edu
Florida	Florida Institute of Technology	Michael Letsky	
	Embry-Riddle Aeronautical University	Ary Glantz	aryjglantz@hotmail.com
Hawaii	University of Hawaii	Wayne Shiroma	cubesat@spectra.eng.hawaii.edu
Illinois	University of Chicago	Geza Gyuk	ggyuk@adlerplanetarium.org
	University of Illinois	Gary Swenson	swenson1@uiuc.edu
Indiana	Purdue University	David Filmer	filmer@ecn.purdue.edu
	Taylor University	Hank Voss	hnvoss@tayloru.edu
	SUNY Geneseo	Josh Reiner	wersing@physics.auburn.edu
Iowa	Iowa State University	Thomas Calgaard	tmichael@iastate.edu
Kansas	University of Kansas	Trevor Sorensen	tsorensen@ku.edu
Lousiana	University of Louisiana	Robert Henry	henry@louisiana.edu
Maryland	US Naval Academy	Bob Bruninga	bruninga@usna.edu
Massachusetts	Dartmouth College	Shaina Damm	
Michigan	Michigan Technological University	Brad King	lbking@mtu.edu

Missouri	Wasington University - St. Louis	Mike Swartwout	mas@mecf.wustl.edu
Montana	Montana State University	David Klumpar	merope@ssel.montana.edu
New York	Cornell University	Mark Campbell	mc288@cornell.edu
	Polytechnic University – NYC	Ximing Li	
New Mexico	New Mexico State University	Stephen Horan	shoran@nmsu.edu
North Carolina	North Carolina State University	Tommy Sebastian	tsebast@ncsu.edu
North Dakota	University of North Dakota	William Semke	william_semke@mail.und.nodak.edu
Oklahoma	University of Oklahoma	Brandon DeKock	
Texas	University of Texas - Austin	Cesar Ocampo	cesar.ocampo@mail.utexas.edu
	Texas Christian University	Andre Mazzoleni	A.Mazzoleni@tcu.edu
	Texas A&M	Diane Hurtado	d-hurtado@tamu.edu
Utah	Utah State University	Chad Fish	
Virginia	George Mason University	Eliud Bonilla	ebonilla@gmu.edu
Washington	University of Washington	Adam Bruckner	Bruckner@aa.washington.edu
Washington D.C.	George Washington University	Jer-Nan Juang	J.JUANG@LaRC.NASA.GOV

Argentina	Universidad de Buenos Aires	Gustavo Fano	
Australia	University of Sydney	Salah Sukkarieh	salah@acfr.usyd.edu.au
Brazil	UNOPAR University	Fernando Stancato	
Canada	Carleton University	Michel Barbeau	barbeau@scs.carleton.ca
	University of Sherbrooke	Jean deLafontaine	Jean.deLafontaine@USherbrooke.ca
	University of Toronto	Robert Zee	rzee@utias-sfl.net
China	Tsinghua University	Li Luming	lilm@tsinghua.edu.cn
Colombia	La Universidad Sergio Arboleda, Bogota Colombia	Cesar Ocampo	cesar.ocampo@mail.utexas.edu
Denmark	Aalborg University, Denmark	Rafal Wisniewski	raf@control.auc.dk
	Technical University of Denmark	Peter Meincke	pme@oersted.dtu.dk
Germany	Fachhochschule Aachen	Artur Scholz	cubesat@fh-aachen.de
	Julius-Maximilians-Universitaet Wuerzburg	Klaus Schilling	schi@informatik.uni-wuerzburg.de
	Technical University of Berlin	Dr. Hakan Kayal	Hakan.Kayal@TU-Berlin.de

	University of Applied Sciences - Weingarten	Klaus Shilling	schi@ars.fh-weingarten.de
	University of Siegen, Germany	Dr. Hubert Roth	roth@rst.e-technik.uni-siegen.de
India	New Delphi	Deepak	daksh@vsnl.net
Turkey	Istanbul Technical University	Dr. A. Rüstem Aslan	aslanr@itu.edu.tr
Italy	University of Trieste, Italy	Anna Gregorio	gregorio@sci.area.trieste.it
	Universita di Roma, Italy	Fabio Santoni	fabio.santoni@uniroma1.it
Japan	Tokyo Institute of Technology, Japan	Saburo Matunaga	Matunaga.Saburo@mes.titech.ac.jp
	University of Tokyo, Japan	Shinichi Nakasuka	nakasuka@space.t.u-tokyo.ac.jp
	Nihon University,Japan	Y. Miyazaki	miyazaki@forth.aero.cst.nihon-u.ac.jp
	Soka University, Japan	Seiji Kuroki	kuroki@ieee.org
Malaysia	University of Malaysia	Faizal Allaudin	taiko2k@hotmail.com
Netherlands	Delft University of Technology	Robbert J. Hamann	R.J.Hamann@LR.TUDelft.NL
Norway	Norwegian University of Science Technology	Egil Eide	eide@tele.ntnu.no
Poland	Warshaw University of Technology	Andrzej Kotarski	andrzej.kotarski@gmail.com
Portugal	Faculdade de Engenharia da Universidade do Porto	Pedro Portela	portela@fe.up.pt
	University of Porto	Tiago Oliveira	em00165@fe.up.pt
Romania	University of Bucharest	Mugurel Balan	mugurel.balan@gmail.com
Saudi Arabia	Beirut Arab University	Rabie Kalash	rkalash@hotmail.com
South Africa	University of Stellenbosch	Arno Barnard	abarnard@sun.ac.za
South Korea	Hankuk Aviation University	Young-Keun Chang	ykchang@mail.hangkong.ac.kr
Spain	La Salle University, Barcelona	Javier Lazaro	jarribas@salleurl.edu
Switzerland	Federal Technical University of Lausanne	Muriel Noca	muriel.noca@epfl.ch
	University of Applied Sciences of Southern Switzerland	Paolo Ceppi	paolo.ceppi@supsi.ch
Taiwan	National Cheng Kung University Taiwan	J.J.	jjmiau@mail.ncku.edu.tw
Turkey	Turkish Air Force Academy	Fuat Ince	fuat.ince@superonline.com
	Bahcesehir University	Cengiz Toklu	yct001@gmail.com
Ukraine	Institute of Technical Mechanics- Ukraine, Dnepropetrovsk	Anatoly Alpatov	alpatov@ukr.net
United Kingdom	Imperial College	Dr. Tim Horbury	t.horbury@imperial.ac.uk
[redacted]			
United States	FunSat - Florida University Collaboration	Kyle Schroedner	funsat@mail.ucf.edu

Europe	European CubeSat Collaboration	Klaus Schilling	schi@informatik.uni-wuerzburg.de
United States	Inland Northwest Space Alliance	Mike Miller	mmiller@inwspace.org
Canada	Win-Cube: MSIG/MAHRCC/Mindset	Stefan Wagener	VE4NSA@amsat.org
	[redacted]		
	Leland High School	Steve Schlink	steveschlink@aol.com
	Saratoga High School	Roxana Safipour	rsafipour@yahoo.com
	Wilcox High School	Lisa Kinneman	kinneman@pacbell.net
Alabama	Auburn University	Luther Richardson	lrich@physics.auburn.edu
	[redacted]		
	South Bay Amateur Radio	Al Rendon	
	StenSat	Ivan Galysh	galysh@juno.nrl.navy.mil
	[redacted]		
Czech Republic	EMP Centauri Ltd.	Marian Vana	info@emp-centauri.cz
Spain	GADESA, Galicia	Manuel Oreiro	manuel.oreiro@ingenierosvigo.com
United States	QuakeFinder	Tom Bleier	tbleier@stellersolutions.com
United States	Tethers Unlimited	Nestor Voronka	voronka@tethers.com
United States	Globaltec R & D Center	Judy Dragich Coenen	globaltec@dmv.com
United States	Global Imaging	Michael Guberek	mguberek@globalimaging.com
United States	Kentucky Science and Technology Corporation	Kris Kimel	kkimel@kstc.com
	[redacted]		
	Pumpkin, Inc.	Andrew E. Kalman	Cubesat Kit

Tethers Unlimited	Nestor Voronka	Subsystems & Modules for CubeSats
Clyde-Space	Craig Clark	Power System & Batteries
Samtec		Connectors
Digi-Key		General Electronics
McMaster-Carr		General Hardware
		General Electronics
Maxim		

[**After 57]**

THIS PAGE INTENTIONALLY LEFT BLANK

APPENDIX B: PARTS

	Description	Manufacturer	Identifier
1	Support Structure	TECO Pneumatics	Drawing #: 8020-5076
2	Roll-in T-nuts	TECO Pneumatics	13032
3	Air Bearing	New Way Air Bearings	POC: Rich Hesse
4	Air Bearing Mount	Custom	¼" Al plates
5	Air Supply Valves/Hoses	American Air Works	POC: Ray Lambert
6	Polycarbonate Parts	Stratasys	NA
7	Linear Motors	New Scale Technologies	SQL-3.4-10
8	Linear Motor Controllers	New Scale Technologies	MC-1100
9	Linear Encoders	New Scale Technologies	Tracker
10	Battery	Inspired Energy	ND2054
11	Battery Manager	Ocean Server	BB-04S
12	DC/DC Converter	Ocean Server	DC123SR
13	PC/104	Advanced Digital Logic	ADLLX8PC – AMD Geode™ LX800
14	Wireless Antenna	D-Link	DWL-G730AP
15	Acrylic Hemisphere	California Quality Plastics	Custom Sphere with inner deck
16	Balance Masses	Custom	Stainless Steel
17	IMU	Analog Device, Inc.	ADIS16405/PCBZ
18	Inclinometers	Rieker	N4

THIS PAGE INTENTIONALLY LEFT BLANK

LIST OF REFERENCES

[1] J. A. Blocker, “TINYSCOPE: the feasibility of a tactically useful, three-axis stabilized, earth-imaging nano-satellite,” M.S. thesis, Naval Postgraduate School, Monterey, California, 2008.

[2] M. D. Van Orden and E. N. Marsh, “Navy Achievements in Satellite Communications,” in *AIAA Communications Satellite Systems Conference*, 1966.

[3] A. J. Butrica, United States, National Aeronautics and Space Administration and History Office, “Beyond the Ionosphere: Fifty Years of Satellite Communication,” Washington, DC: National Aeronautics and Space Administration, NASA History Office, 1997.

[4] D. I. Dalgleish, “An Introduction to Satellite Communications,” London: P. Peregrinus on behalf of the Institute of Electrical Engineers, 1989.

[5] R. R. Jacobson and T. Linkabit, “Naval UHF SATCOM terminal programs: AN/WSC-3 and Mini-DAMA,” in *Space Programs and Technologies Conference*, 1994. Available: http://www.aiaa.org.libproxy.nps.edu/content.cfm?pageid=406 (accessed September 2009).

[6] P. S. Melancon and R. D. Smith, “Fleet Satellite Communications (FLTSATCOM) Program,” in *8th Communications Satellite Systems Conference,* 1980. Available: http://www.aiaa.org.libproxy.nps.edu/content.cfm?pageid=406 (accessed September 2009).

[7] Space Systems Company, Lockheed Martin Corporation. “Mobile User Objective System (MUOS),” July 2009, http://www.lockheedmartin.com/products/muos/index.html (accessed September 2009).

[8] U.S. Navy RDTEN Budget Item Justification (February 2007), 2009, p. 40. Available: http://www.dtic.mil/descriptivesum/Y2008/Navy/0303109N.pdf (accessed September 2009).

[9] National Reconnaissance Office, “Corona facts,” July 2009, http://www.nro.gov/corona/facts.html (accessed September 2009).

[10] C. J. Hrbek, J. A. Cestone, E. J. St. George and R. L. Greenspan. Underwater Navigation, July 2009. Available: http://www.accessscience.com.libproxy.nps.edu/content.aspx?id=720700 (accessed September 2009).

[11] G. Flessate (private communication), July 2009.

[12] Wikipedia, "Automatic Identification System," July 2009, http://en.wikipedia.org/wiki/Automatic_Identification_System (accessed September 2009).

[13] U.S. Government Printing Office. (October 2009). Code of Federal Regulations Title 27 Part 80.5: Definitions. Available: http://edocket.access.gpo.gov/cfr_2002/octqtr/pdf/47cfr80.5.pdf (accessed September 2009).

[14] U.S. Coast Guard Navigation Center, "AIS Messages." November 2009, http://www.navcen.uscg.gov/enav/ais/AIS_messages.htm (accessed September 2009).

[15] ORBCOMM, "Company Information," July 2009, http://www.orbcomm.com/about/companyInfo.htm (accessed September 2009).

[16] ORBCOMM, "Satellite M2M," July 2009, http://www.orbcomm.com/solutions/satelliteM2M.htm (accessed September 2009).

[17] Small Satellites Home Page, "Satellite Classification," October 2009, http://centaur.sstl.co.uk/SSHP/sshp_classify.html (accessed September 2009).

[18] NASA Goddard Space Flight Center, "Nanotech Vs. Nanosat: A Small Introduction", 30 April 2007, http://gsfctechnology.gsfc.nasa.gov/FeaturedArchiveSatVtech.html (accessed September 2009).

[19] Cubesat.org, "CubeSat Design Specifications," December 2009, http://cubesat.org/images/developers/cds_rev12.pdf (accessed September 2009).

[20] L. David, "Cubesats: tiny spacecraft, huge payoffs," December 2009, Space.com. Available: http://www.space.com/businesstechnology/cube_sats_040908.html (accessed September 2009).

[21] Cubesatkit.com, “Price List,” December 2009, http://www.cubesatkit.com/ (accessed September 2009).

[22] D. Levy, “First anniversary of student-built satellite in space,” Stanford New Service, 30 January 2001. Available: http://news.stanford.edu/pr/01/opal131.html (accessed September 2009).

[23] D. A. Vallado and W. D. McClain, Fundamentals of Astrodynamics and Applications, 3rd Ed. New York: Springer, 2007.

[24] J. J. Sellers, W. J. Astore, K. S. Crumpton, C. Elliot, R. B. Giffen, “Understanding Space: An Introduction to Astronautics,” San Francisco: McGraw-Hill, Inc., 1994.

[25] J. L. Crowley, Y. Demazeau, “Principles and techniques for sensor and data fusion,” Signal Processing, Vol. 32, No. 1-2, May 1993, pp. 5–27. Available: http://www-prima.inrialpes.fr/Prima/Homepages/jlc/papers/SigProc-Fusion.pdf (accessed September 2009).

[26] Wikipedia, “Attitude dynamics and control,” December 2009, http://en.wikipedia.org/wiki/Attitude_dynamics_and_control (accessed September 2009).

[27] G. A. Smith. Dynamic Simulators for Test of Space Vehicle Attitude Control Systems, in *Virginia Polytechnic Institute Proceedings of the Conference on the Role of Simulation in Space Technologies*, 1964.

[28] J. L. Schwartz, M. A. Peck, C. D. Hall, “Historical review of air-bearing spacecraft simulators,” *Journal of Guidance, Control and Dynamics*, vol. 26, no. 4, July-August 2003.

[29] R. J. Twiggs, J. Jung, N. Kuzuya, J. Alvarez, “The Design of the OPAL Attitude Control System,” Space Systems Development Laboratory, Stanford University, Stanford, California, 1996.

[30] Small Satellite Home Page, “2000,” December 2009, http://centaur.sstl.co.uk/SSHP/micro/micro2000.html (accessed September 2009).

[31] C. O. Mittelsteadt and E. A. Mehiel, “The cal poly spacecraft attitude dynamics simulator - CP/SADS,” in *AIAA Guidance, Navigation and Control Conference and Exhibit*, 2007.

[32] S. F. Silva (private communication), November 2009.

[33] J. L. Schwartz and C. D. Hall. The Distributed Spacecraft Attitude Control System Simulator: Development, Progress, Plans." in *2003 Flight Mechanics Symposium*, 2003. Available: http://www.aoe.vt.edu/%7Ecdhall/papers/FMS03.pdf (accessed September 2009).

[34] J. J. Kim, B. N. Agrawal. "Automatic mass balancing of air-bearing-based three-axis rotational spacecraft simulator," Journal of Guidance, Control, and Dynamics, vol. 32, no. 3, May–June 2009.

[35] Q. Young (private communication), 2009.

[36] D. Jung, P. Tsiotras, "A 3-DoF experimental test-bed for integrated attitude dynamics and control research," in *AIAA Guidance, Navigation, and Control Conference and Exhibit,* 2003.

[37] J. W. Kim, R. Cristi and B. N. Agrawal. "Attitude Determination for NPS Three-Axis Spacecraft Simulator," in *2004 AIAA/AAS Astrodynamics Specialist Conference and Exhibit*, 2004. Available: http://www.nps.edu/Academics/Centers/SRDC/Docs/AIAA-2004-5386-624-kim_cristi_agrawal.pdf (accessed September 2009).

[38] J. J. Kim and B. N. Agrawal. "System identification and automatic mass balancing of ground-based three-axis spacecraft simulator," in *AIAA Guidance, Navigation, and Control Conference and Exhibit*, 2006. Available: http://www.nps.edu/Academics/Centers/SRDC/Docs/AIAA-2006-6595-550-kim_agrawal.pdf (accessed September 2009).

[39] F. D. Roe, D. W. Mitchell, B. M. Linner, D. L. Kelley. "Simulation techniques for avionics systems – An introduction to a world class facility," AIAA Meeting Papers on Disc, 1996, pp. 535–543.

[40] Wikipedia, "Moore-Penrose psuedoinverse," December 2009, http://en.wikipedia.org/wiki/Moore–Penrose_pseudoinverse (accessed September 2009).

[41] Design World Staff, "Stratasys FDM 400mc Prototyping Machine," 8 November 2009, http://www.stratasys.com (accessed September 2009).

[42] New Way Air Bearings, (private communications), June 2009.

[43] New Way Air Bearings, "Porous Media Technology," November 2009, http://www.newwayairbearings.com/Porous-Media-Technology (accessed September 2009).

[44] J. Bondoc (private communication), October 2009.

[45] 80/20 Product Catalog, 80/20® Inc., Columbia City, Indiana, p. 502, December 2009. Available: http://www.8020.net (accessed September 2009).

[46] Fortus 3D Production Systems, “PC (polycarbonate) for FORTUS 3D Production Systems,” December 2009.

[47] Advanced Digital Logic Product Datasheet, “ADLLX8PC - AMD Geode™ LX800,” November 2009, San Diego, California, Available: http://www.adl-usa.com/products/cpu/datasheets/ADLLX8PC.pdf (accessed September 2009).

[48] “Diamond-MM-32-AT User Manual,” Diamond Systems Corporation, Newark, CA, December 2009.

[49] Digi-Key, Corporation, Product Datasheet, “ADIS16405/PCBZ-ND,” November 2009, Available: http://www.analog.com/static/imported-files/data_sheets/ADIS16405.pdf (accessed September 2009).

[50] Rieker, Inc., “Electronic Inclinometer: N Series,” November 2009. Available: http://www.riekerinc.com/E-Inclinometers/SeikaPDF/N_BrochW.pdf (accessed September 2009).

[51] Sinclair Interplanetary, “SS-411 Digital Sun Sensor Interface Control Document,” December 2009, http://www.sinclairinterplanetary.com/digitalsunsensors

[52] Spica Technologies Corporation, “Digital Motion Analysis System”, November 2009. Available: http://www.spicatek.com/ (accessed September 2009).

[53] J. Mikael Brommels, (private communication), November 2009.

[54] New Scale Technologies, Inc., “SQUIGGLE Micro Motors for OEMs,” November 2009, http://www.newscaletech.com/doc_downloads/SQL-3-4_Motor_datasheet.pdf (accessed September 2009).

[55] J. Prado, G. Bisiacchi, L. Reyes, E. Vicente, F. Contreras, M. Mesinas, and A. Juárez. “Three-axis air-bearing based platform for small satellite attitutde determination and control simulation,” *Journal Applied Research and Technology*, vol. 3, no. 003, Universidad Nacional Autónoma de México, pp. 222–237.

[56] Firgelli Technologies Inc., (private communication), November 2009.

[57] P. Healy, “Mass Property System Identification of a Spacecraft Simulator,” M.S. thesis, California Polytechnic State University, San Luis Obispo, California, 2006.

[58] Cubesat.org, “Participants”, November 2009, http://cubesat.atl.calpoly.edu/pages/satellite-developers.php (accessed September 2009).

INITIAL DISTRIBUTION LIST

1. Defense Technical Information Center
   Ft. Belvoir, Virginia

2. Dudley Knox Library
   Naval Postgraduate School
   Monterey, California

3. Marcello Romano
   Naval Postgraduate School
   Monterey, California

4. Riccardo Bevilacqua
   Naval Postgraduate School
   Monterey, California

5. Mark Meissner
   Wauwatosa, Wisconsin

6. Larry Calahan
   Davenport, Iowa

7. Michael Gawenka
   Bremerton, Washington